Title: Microglia mediate contact-independent neuronal pruning via secreted Neuraminidase-3 associated with extracellular vesicles

Authors: Corleone S. Delaveris,[1] Catherine L. Wang,[1] Nicholas M. Riley,[1] Rishikesh U. Kulkarni,[1‡] Carolyn R. Bertozzi[1,2‡]

Affiliations:
[1]Stanford University, Department of Chemistry and Sarafan ChEM-H, Stanford, CA 94305, USA
[2]Howard Hughes Medical Institute, Stanford, CA 94305 USA
[‡]To whom correspondence should be addressed: rishi@kulkarni.science; bertozzi@stanford.edu

Abstract: Neurons communicate with each other through electrochemical transmission at synapses. Microglia, the resident immune cells of the central nervous system, can prune these synapses through a variety of contact-dependent and -independent means. Microglial secretion of active sialidase enzymes upon exposure to inflammatory stimuli is one unexplored mechanism of pruning. Recent work from our lab showed that treatment of neurons with bacterial sialidases disrupts neuronal network connectivity. Here, we find that activated microglia secrete Neuraminidase-3 (Neu3) associated with fusogenic extracellular vesicles. Furthermore, we show Neu3 mediates contact-independent pruning of neurons and subsequent disruption of neuronal networks through neuronal glycocalyx remodeling. We observe that *NEU3* is transcriptionally upregulated upon exposure to inflammatory stimuli, and that a genetic knock-out of *NEU3* abrogates the sialidase activity of inflammatory microglial secretions. Moreover, we demonstrate that Neu3 is associated with a subpopulation of extracellular vesicles, possibly exosomes, that are secreted by microglia upon inflammatory insult. Finally, we demonstrate that Neu3 is both necessary and sufficient to both desialylate neurons and decrease neuronal network connectivity. These results implicate Neu3 in remodeling of the glycocalyx leading to aberrant network-level activity of neurons, with implications in neuroinflammatory diseases such as Parkinson's disease and Alzheimer's disease.

Keywords: microglia, neuraminidase, neuronal network, Neuraminidase-3, neurons, voltage imaging, neuroinflammation, glycocalyx

Introduction.

The brain is made of a vast interconnected and interdependent network of neurons, communicating information through synapses. Microglia, the resident immune phagocytes of the central nervous system, prune these synapses through several mechanisms, including direct and complement-mediated phagocytosis.[1–7] These activities are upregulated in the context of neuroinflammatory pathologies, including Alzheimer's disease and Parkinson's disease.[8–10] However, the specific mechanisms by which hyperinflammatory microglia mediate these effects remain unclear, especially in the context of how these actions impact neuronal networking and communication through synapses. Given that neurodegenerative diseases correlate with aberrant network-level neuronal activity,[9,10] it is important to understand the molecular mechanisms by which inflammatory microglia regulate neuronal communication.

Neuroinflammation has been correlated with changes in the glycocalyx – the coating of sugars on cell surfaces – of both neurons and microglia.[11–15] Sialic acids are a particular subset of bioactive sugars in the glycocalyx. They are known to modulate neuronal excitability and plasticity,[7,16] and changes in sialylation state are associated with neuroinflammation and microglial activation.[16–22] Upon exposure to inflammatory stimuli, microglia have been observed to release sialidase activity into the surrounding media, which effects desialylation,[17,22,23] deposition of opsonizing factors,[18,23] microglial activation,[16,23] and phagocytosis of neurons.[17,23] Additionally, our lab has recently identified sialylation state as a critical factor in maintaining neuronal excitability and network integration.[21] Collectively, these observations point to the glycocalyx as a regulator of neuronal activity.

Herein, we tested the hypothesis that sialidases released by microglia could affect contact-independent neuronal pruning. We found that the peripheral membrane glycolipid sialidase Neuraminidase-3 (Neu3) is secreted by microglia upon activation by inflammatory stimuli. Neu3 was localized to a population of extracellular vesicles that are fusogenic with neurons. Using a voltage-sensing imaging dye, we found Neu3 is both necessary and sufficient to mediate neuronal pruning and the disconnection of neuronal networks. Based on these data, we propose a mechanism in which microglia secrete Neu3 to remodel neuronal glycocalyces to modulate neuronal connectivity. These results have implications for how neuroinflammation results in neuronal network dysfunction.

Results and Discussion.

Activated microglia upregulate *NEU3* and require *NEU3* to desialylate neuronal glycocalyces

We and others have observed that microglial secretions possess sialidase activity and are capable of desialylating model cell lines[24] and primary neurons (**Figure 1a,b**). Notably, these effects can be pharmacologically inhibited with zanamivir, which has inhibitory activity for human sialidases.[25] Of the four mammalian sialidases, three have reported expression in the brain.[26] To identify the sialidase(s) secreted by activated microglia responsible for this activity, we activated BV-2 murine microglia using lipopolysaccharide (LPS) and assessed relative mRNA expression of sialidase genes using qPCR. We observed a 50% increase in *NEU3* transcripts following activation (p=0.041) and statistically insignificant changes in *NEU1* and *NEU4* (p=0.11 and p=0.90, respectively) (**Figure 1c**). To investigate the role of the glycolipid sialidase Neu3[27] in desialylating neurons, we generated *NEU3* (the gene encoding Neu3) knockout (KO) BV-2 microglia and compared the sialidase activity of wild-type (WT) and *NEU3* KO BV-2 secretions (**Figure S1**). *NEU3* KO conditioned media exhibited minimal sialidase activity compared to WT (p=0.043), as measured by Peanut Agglutinin (PNA) binding of terminal N-acetylgalactosamine exposed by desialylation on neuronal membranes (**Figure 1d**). Consistent with the observation that Neu3 is predominantly a glycolipid (e.g., ganglioside) sialidase,[27–30] we did not observe significant changes in sialylated glycoproteins of neurons treated with conditioned media from WT versus *NEU3* KO microglia (**Table S1**).

As prior studies have implicated Neu1 translocation and desialylation in cis as a critical component of microglial activation,[14,15,23] we sought to determine whether the loss of secreted sialidase activity in *NEU3* KO BV-2 cells was a consequence of impaired inflammatory activity. We observed that *NEU3* KO cells had impaired autodesialylation in response to LPS treatment compared to WT as measured by periodate labeling of sialic acids (p=0.51 and =0.038, respectively), but that both WT and *NEU3* KO cells upregulated TNF□ to similar levels in (WT, *p*=0.002; *NEU3* KO, *p*=0.02) (**Figure S2**). Therefore, *NEU3* KO cells are still able to secrete inflammatory signals. TNF□ secretion in both cell lines was inhibited by the pan-sialidase inhibitor deoxy-2,3-anhydroneuraminic acid (DANA), consistent with previous observations with Neu1.[14,23] Given that the BV-2 microglia are still capable of secreting inflammatory molecules, the autodesialylation likely does not have a biological impact in this context. Moreover, these data implicate Neu3 as the secreted sialidase, rather than an upstream component.

Microglial secreted Neu3 is associated with extracellular vesicles that fuse with neurons

Neu3 has been shown to behave as a peripheral membrane protein,[31] with recent studies demonstrating that the enzyme is S-acylated.[32] Additionally, microglia are known to secrete extracellular vesicles (EVs) upon activation.[33] Therefore, we hypothesized that Neu3 might be secreted in association with EVs. To investigate this hypothesis, we isolated EVs from resting and activated microglia conditioned media using commercial lectin-based isolation kits. We confirmed that we were isolating EVs based on proteomics of the surfaceome, which identified known EV proteins, but we were unable to detect Neu3 directly (**Figure S3**, **Table S2**). To confirm that Neu3 colocalizes with EVs, we inserted a 3xFLAG-tag at on the endogenous NEU3 gene by homology-directed recombination (**Figure S4**). We then performed an immunocapture bead assay in which magnetic beads were functionalized with anti-murine CD63 to capture EVs and incubated with microglia-conditioned medium. Captured EVs were analyzed with anti-FLAG and either anti-CD9 or anti-CD81, both of which are used as EV markers.[34] We observed a FLAG-positive population of EVs, the relative population of which significantly increased upon LPS-stimulation, suggesting that microglial Neu3 is secreted via EVs upon immune stimulus (**Figure 2a, S5**).

To confirm that EV-resident Neu3 is responsible for the sialidase activity on neurons, we treated neurons with EV-enriched or EV-depleted microglia conditioned media. We observed that EV-enriched fractions demonstrated significantly increased sialidase activity compared to EV-depleted fractions (*p*=0.023, **Figure 2b**), suggesting that EVs are responsible for desialylation. Consistent with this, pharmacological inhibition of extracellular vesicle production with GW4869[35] decreased sialidase activity of the enriched fraction (*p*=0.014, **Figure 2c**). Furthermore, upon staining EVs with a membrane dye we observed robust dye transfer to neuronal membranes, indicating vesicle fusion with neurons (*p*=0.044, **Figure 2d**). These data suggest a model in which microglia expel extracellular vesicles containing Neu3, which fuse with neuronal membranes and cause desialylation of the extracellular leaflet.

Secreted Neu3 disrupts neuronal network integration in primary neurons

Our lab has recently demonstrated that desialylation of primary neurons in culture by the highly promiscuous *Arthrobacter ureafaciens* (Au) sialidase results in decreased cell surface sialic acids and neuronal network integration.[21] We hypothesized that Neu3 would have a similar effect. To assay this, we performed voltage imaging of primary neurons in culture using BeRST1,[36] a membrane-localized voltage-sensitive fluorophore (**Figure 3a,b**). This technique enables simultaneous high-quality measurements of membrane potential in larger groups of neurons compared to traditional electrophysiology, enabling studies of network connectivity by comparing when multiple neurons in a given field of view fire.[36] We have previously used this method in combination with factor analysis to quantify neuronal network connectivity as the “shared variance” of the network.[21] In brief, covariance in the firing activity of measured neurons may reflect variation in synaptic input (factors), while unexplained variance reflects the fraction of the neuron’s activity that arises spontaneously. It

follows then that the ratio of shared variance to total variance measures how much of a neuron's activity is network-driven.

Using voltage imaging, we found that neurons treated with enriched EVs from activated BV-2 microglia exhibited a markedly lower firing rate compared to resting BV-2 microglia (-1.7 Hz, p=0.048), an effect that could be pharmacologically rescued with GW4869 (**Figure 3c**). Analyzing the data using factor analysis to quantify network connectivity, as we have previously described,[21] we found that neuronal networks treated with activated microglial EVs experienced a substantial 29% decrease in average per-neuron shared variance compared to EVs from resting microglia (p=0.015). This indicates that the integration of measured neurons into a network had been significantly disrupted by treatment. This effect was rescued by pharmacological inhibition of EV production with GW4869 (p=0.029) (**Figure 3d**). These results indicate that activated microglial EVs are necessary and sufficient to disrupt synaptic communication.

To isolate the effects of Neu3 over other potential regulatory components of microglial secreted EVs, we overexpressed Neu3 in HeLa cells, which have been previously described to secrete Neu3 on the exterior surface of microvesicles and exosomes upon overexpression of *NEU3*.[37] We transiently transfected HeLa cells with plasmids encoding either wild-type Neu3 or a catalytically inactive point mutant (Y369F) (**Figure S6**) and enriched EVs from the conditioned media as we did with the BV-2 conditioned media. Using periodate labeling, we observed that these EV-enriched fractions were still capable of desialylating neuronal membranes (**Figure S7**), suggesting that Neu3 is the sialidase remodeling the neuronal glycocalyces in microglial secretions. Using voltage imaging, we observed that neither wild-type or Y369F Neu3 containing HeLa-derived EV's caused significant changes in firing rate (WT: -0.26 Hz, p=0.58; Y369F: -0.14 Hz, p=0.65), indicating that the observed decrease in firing rate of neurons treated with EV's from activated microglia is likely due to secreted factors besides of Neu3 (**Figure 3e, S8**). However, factor analysis revealed a 15% decrease in per-neuron shared variance between WT and Y369F-treated cultures (p=0.046), indicating a Neu3 activity-dependent loss of connectivity (**Figure 3f**). Congruent with this, pharmacological inhibition of Neu3 with DANA abrogated the effect of wild-type Neu3 on neuronal connectivity in culture but had no significant effect in Y369F-treated cultures (WT, p=0.028; Y369F, p=0.48; **Figure 3f**). This observation demonstrates that EV-associated Neu3 activity alone is sufficient to drive changes in neuronal communication, a previously unknown function of Neu3.

Conclusions

The prototypical sialic acid, 5-*N*-acetylneuraminic acid, was named based on the observed abundance of sialic acids on the external leaflet of neurons, particularly sialylated glycolipids known as gangliosides.[38] Neu3 is a membrane-associated glycolipid sialidase[28] that we speculated might play a role in regulating neuronal connectivity. The data herein present a new mechanism by which microglia regulate neuronal sialylation by secretion and transfer of Neu3 via extracellular vesicles. Moreover, we show that Neu3-mediated remodeling has a dramatic impact on the connectivity of neuronal networks, providing molecular detail for a contact-independent mechanism of neuronal pruning. These findings demonstrate a novel axis by which microglia and neurons communicate. Indeed, sialoglycans may serve as a mechanistic bridge between neuroinflammation and downstream changes in electrophysiology, which would position them as potential therapeutic targets for neurological disorders. The electrical mechanism of this rewiring, as well as other neuroinflammatory signals that lead to this effect, are exciting grounds for future research.

Acknowledgements.

This work was supported by National Institutes of Health Grant GM058867. C.S.D. was supported by a National Science Foundation Graduate Research Fellowship DGE-114747 and a Stanford Interdisciplinary Gradate Fellowship affiliated with ChEM-H. N.M.R. was funded by National Institutes of Health Grant K99GM147304. Figure illustrations were created using BioRender.com.

Competing Interests.

C.R.B. is a co-founder and Scientific Advisory Board member of Lycia Therapeutics, Palleon Pharmaceuticals, Enable Bioscience, Redwood Biosciences (a subsidiary of Catalent), InterVenn Bio, GanNa Bio, OliLux Bio, Neuravid Therapeutics, Valora Therapeutics, and Firefly Bio, and is a member of the Board of Directors of Alnylam Pharmaceuticals and OmniAb. R.L.K. is a co-inventor on a patent related voltage-gated imaging dyes.

Materials and Methods.

Cell culture

BV2 murine microglia (a kind gift from T. Wyss-Coray) were propagated in DMEM supplemented with 10% hiFBS. Microglia were maintained at a low passage number (< 10 since obtaining initial stocks) and split at or before ~ 70% confluency to avoid runaway inflammation as caused by dead or floating BV2 cells. If cells grew overconfluent, the culture was discarded. Typically, ~ 1e6 microglia were seeded in a T75 in 25 mL split every two days. Microglia were harvested using Gibco enzyme-free dissociation buffer, incubated for 5 min at room temperature, and lifted with gentle tapping and pipetting. Microglia were diluted in an equal volume of complete media, counted with a hemocytometer, pelleted by centrifugation (300 rcf, 5 min), and resuspended in complete media for subculturing.

HeLa cells (ATCC CCL-2) were propagated in DMEM supplemented with 10% hiFBS. HeLa cells were subcultured at a confluence below 80% to avoid overgrowth. Typically, HeLa cells were split 1:5 every two to three days. HeLa cells were lifted using trypsin and pelleted by centrifugation (300 rcf, 5 min), before resuspending in fresh media.

Preparation of microglia-conditioned media

Low passage and subconfluent BV2 microglia were harvested using Gibco enzyme-free dissociation media, incubated for 5 min at room temperature, and lifted with gentle tapping and pipetting. Microglia were diluted in an equal volume of complete media, counted with a hemocytometer, pelleted by centrifugation (300 rcf, 5 min), and resuspended in NB++ media (PN) for subculturing.

Cultures for conditioned media were seeded at 4e4 cells per cm^2 at 2e5 cells per mL. In some cases, microglia were stimulated with LPS (1 µg/mL). Cells were cultured at 37 °C in 5% CO_2 for 18 h. The media was then harvested with careful pipetting cleared of floating cells and large debris by centrifugation (500 rcf, 5 min). The clarified media was then transferred to a clean tube. In some cases, 5-N-acetyl-2,3-dehydro-2-deoxyneuraminic acid (DANA) was added to 2 mM. An equal volume of conditioned media was then added to neuronal cultures.

Transfection of HeLa cells and conditioning of media

HeLa cells were transfected with plasmids encoding murine Neu3 (wt or the catalytically inactive mutant Y369F) using Transit2020 according to the manufacturer's protocol. Plasmids were custom ordered from Twist Biosciences encoding murine Neu3 (wt or Y369F) C-terminally tagged with a short linker (GSGGGSGGGGSG) followed by a 3xFLAG tag. Constructs were optimized for human codons and cloned into a pCMV vector from Twist. After 24 h, the cells were washed with OptiMEM and cultured in a low-volume of OptiMEM for an additional 24 h, at which point conditioned media was harvested and EV's were isolated.

Isolation and labeling of extracellular vesicles

Media was prepared as described above in 25 mL of media in a T125 cell culture flask. In some cases, bulk extracellular vesicles were isolated by concentrating media in a 100 kDa spin-filter. In other cases, exosomes were specifically isolated from conditioned media using Takara Capturem EV spin columns (Takara, 635723) according to the manufacturer's instructions.

For extracellular vesicle labeling experiments, BV-2 microglia were cultured in T25 flasks in 5 mL of Dulbecco's modified eagle medium (DMEM; Gibco) and activated overnight with LPS (1 µg/mL). Supernatant was isolated and incubated with PKH67 dye for 15 minutes at 37 °C following the PKH67GL-1KT kit (Sigma)[19]. Extracellular vesicles were then isolated as described above and resuspended in Neurobasal media (Gibco) with 1% GlutaMAX and 2% B-27 supplement. Primary hippocampal neurons were treated overnight with dyed EV preparation and imaged following kit instructions.

GW4869 treatment of microglia

GW4869 (#D1692, Sigma) was dissolved in DMSO to make a stock solution of 0.2 mg/mL. For inhibition of exosome generation, BV-2 microglia were treated for 3 µM GW4869 for 24 hours before 24-hour LPS treatment. Culture supernatants were collected for exosome isolation and neuronal treatment.

Periodate labeling of cell surface sialosides

Cells were washed with HBSS solution (Gibco) and then incubated with 1 mM sodium (meta)periodate ($NaIO_4$; Sigma) in DPBS (Sigma) for 30 minutes on ice. Cells were then washed twice with sodium acetate buffer (pH 4.7) and fixed for 10 minutes in a 1:1 acetate buffer:methanol solution on ice, then fixed for 10 min in pure methanol. Cells were then washed with sodium acetate buffer and incubated with AlexaFluor 488 hydroxylamine dye (25 uM in sodium acetate buffer; Thermo) for 1 hour at 4 Celsius. Imaging was performed on an Axio Observer Z-1 (Zeiss) equipped with a Spectra-X Light engine LED light (Lumencor), controlled with Micro-Manager. Images were acquired with a Plan-Apochromat 20x/0.8 air objective (Zeiss) paired with image capture from the ORCA-Flash4.0 sCMOS camera (sCMOS; Hamamatsu). Dye was excited with cyan LED 470/24 nm) and emission was collected after passing through the Zeiss 90 HE filter set (425/30 nm, 514/30 nm, 592/25 nm, 709/100 nm LP).

Generation of CRISPR KO of mNeu3

Plasmid constructs encoding Cas9 and a sgRNA were prepared in the lentiCRISPRv2 vector according to published protocols.[39] Guides were selected based on the genome-wide guides described by Bassik and coworkers.[40] Plasmid-bearing Stbl3 *E. coli* were grown in 50 mL cultures and DNA was extracted and endotoxin purified by MiraPrep.[41]

LentiCRISPRv2 plasmids were packaged in lentiviruses produced from HEK293Ts cotransfected with pGag/Pol, pRev, pTat, and pVSVG (gift from the Yi-Chang Liu and Jonathan Weismann). In brief, 1.5 µg of LentiCRISPRv2 plasmid were combined with 0.1 µg of each packaging plasmid and Lipofectamine LTX (Thermo Fisher, 15338100) in OptiMEM (Thermo Fisher, 31985062). Transfection complexes were added to HEK293Ts at 70-80% confluency in a 6 well plate in 2 mL fresh media. The media was aspirated after 12 h and bleached. After 48 h, the media was harvested and filtered through a 0.45 µm syringe filter to afford the viral supernatants.

BV2 cells were resuspended in fresh viral-containing media with polybrene (8 µg/mL). Media was changed after 24 h, and after 72 h antibiotic selection was started (2.5 µg/mL). After two weeks of selection, editing of the target gene was validated by TIDE analysis.[42]

Cytokine release assay

Adherent NEU3 KO and WT BV-2 microglia were plated (100,00 cells/well in a 24-well plate) in Neurobasal media (Gibco) with 1% GlutaMAX and 2% B-27 supplement one day prior to experiment. Media was treated with LPS (1 µg/mL), LPS + DANA (2 µM), or left untreated during plating. Three technical replicates were made per treatment. After 24 hours, cells were spun down at 500 rcf for 5 minutes to remove debris, and supernatant was extracted for analysis. Cytokine levels were assessed using the BD Cytometric Bead Array

(CBA) Mouse Inflammation Kit. Flow cytometry was performed on a BD Accuri C6 Plus, and FlowJo software was used to gate on single cells and live cells for analysis.
µL

Generation of endogenous tagging of mNeu3 by homology-directed recombination

Endogenous tagging of murine Neu3 in BV2 cells was achieved using the Mendenhall-Myers system.[43] In brief, a pFETCh donor plasmid (Addgene, 63934) containing homology arms for mNeu3 (see table of gene fragments) was prepared along with PX458 plasmids containing one the only potential target cut site for mNeu3, as outlined by the target selection described by Mendenhall and Myers. Plasmids were prepared from 50 mL cultures of Stellar *E. coli* and purified by MiraPrep.[41]

Low passage BV2 microglia were transfected by magnetofection (OZ Biosciences) according to the manufacturer's protocols. After 48 h, microglia were treated with a low dose of antibiotic selection (G418, 200X). After two weeks of treatment, only the cells co-transfected with pFETCh donor and PX458 bearing the sgRNA were alive and growing well in the presence of G418 (0.25 mg/mL). The polyclonal population was grown out and the genomic DNA was isolated using a GeneJET Genome DNA Purification Kit (Thermo). PCR was performed using primers +/- 750 bp of the insertion site and compared to PCR products from wt cells. A clear 2.5 kbp band was observed in addition to a 1.5 kbp band of comparable intensity, indicating (mostly) monoallelic insertion of the transfer gene.

Extracellular vesicles bead capture and analysis by flow cytometry

Immunocapture beads for murine extracellular vesicles were prepared by conjugating polyclonal anti-murine CD63 (ThermoFisher, PA5-100713) to tosyl-functionalized M450 Dynabeads according to the manufacturer's protocol for antibody conjugation. After antibody conjugation, the beads were blocked with excess BSA and quenched in pH 8.5 TBS before use.

BV2-conditioned media was cleared by centrifugation (500 rcf, 5 min) and immunocaptured overnight with 2e6 anti-mCD63 beads/mL at 4 °C in a rotating Eppendorf. The beads were magnet captured and washed with cold 0.1% BSA in PBS. EV-bead complexes were stained at 2e6 beads/mL with antibody solutions for 1 h at room temperature protected from light. Antibodies were used at the following dilutions: anti-mCD9 clone KMC8 PE conjugate (ThermoFisher 12-0091-81, 1:50); anti-mCD81 clone Eat2 PE conjugate (BD Biosciences 559519, 1:50); anti-FLAG clone D6W5B AlexaFluor 647 conjugate (Cell Signaling Technologies 15009S, 1:50); rat IgG2a isotype control PE conjugate (BD Biosciences 554689, 1:50); rabbit IgG isotype control AlexaFluor 647 conjugate (ThermoFisher 51-4616-82, 1:50). Beads were magnet captured, washed, resuspended at 1e6 beads/mL and analyzed by flow cytometry on an Accuri C6 flow cytometer. Data were analyzed in FlowJo. Beads were gated on isotype-treated controls.

Quantitative reverse transcriptase PCR analysis

Expression levels of Neu1, Neu3, and Neu4 in murine BV2 microglia and primary murine hippocampal neurons were evaluated by quantitative RT-PCR (qPCR). Total RNA was isolated by TRIzol reagent extraction (ThermoFisher, 15596026) and Zymo RNA Clean and concentrator kits (Zymo, R1013) using manufacturer's protocols. Libraries of cDNA were generated via EcoDry premix kit (Takara, 639542) using 2 µg total RNA. Transcript levels were quantitated via qPCR using SybrGreen master mix (ThermoFisher, 4309155). Transcript levels were normalized to transcript levels of glyceraldehyde-3-phosphate dehydrogenase (GAPDH).

Dissociated hippocampal cultures

All animal procedures were approved by Stanford University's Administrative Panel on Laboratory Animal Care and conformed to the NIH Guide for Care and Use of Laboratory Animals and the Public Health Policy. Primary hippocampal tissue was harvested from E16.5 C57BL/6 embryonic mice (Charles River) immediately after sacrifice of the pregnant dam. The isolated hippocampi were dissociated using Papain Dissociation System

(Worthington Biochemical Corporation) and trituration with fire-polished Pasteur pipettes. The dissociated cells were plated onto 12mm coverslips (Chemglass Life Sciences) pre-treated with Poly-D Lysine (PDL; 1 mg/mL, Sigma-Aldrich) at a density of 6□×□104 cells per coverslip. The cells were maintained for 24 hours in Dulbecco's modified eagle medium (DMEM; Gibco) supplemented with 4.5 g/L D-glucose, 10% FBS, 1% GlutaMAX, and 2% B-27 (Gibco), and then switched to Neurobasal media (Gibco) with 1% GlutaMAX and 2% B-27 supplement. Plates were incubated at 5% CO2, 37°C, and subsequent media changes took place every 7 days.

Voltage imaging of neurons

Neurons were incubated with an HBSS solution (Gibco) containing BeRST1 (1.0µM; Miller Lab, UC Berkeley) for 20 minutes at 37°C prior to imaging. Functional imaging of hippocampal cells was performed on an Axio Observer Z-1 (Zeiss) equipped with a Spectra-X Light engine LED light (Lumencor), controlled with Micro-Manager. Images were acquired with a Plan-Apochromat 20x/0.8 air objective (Zeiss) paired with image capture from the ORCA-Flash4.0 sCMOS camera (sCMOS; Hamamatsu) with 4x4 in-camera binning. We used a sampling rate of 0.5 kHz over 5 or 10 seconds in order to resolve individual action potentials. To achieve maximum sampling rate, a field of view (FOV) size of 512x100 pixels (665.6x130 µm) was used for simultaneous recording of 5-15 neurons at a time. BeRST 1 was excited with a 631 nm light (LED; 631nm, 28 nm bandpass) with an LED power of 70%. Emission from BeRST 1 was collected with a 680/10 nm bandpass emission filter after passing through a dichroic mirror (425/30 nm, 514/30 nm, 592/25 nm, 709/100 nm LP).

Image analysis

Analysis of voltage traces in primary neurons was performed using ImageJ and custom Python scripts. All Python scripts used to analyze data in this study are available at github.com/rishi-kulkarni/SpykeMapper. Regions of interest (ROIs) were drawn around cell bodies within a field of view and the average fluorescence over time was extracted and inputted into an Excel workbook. The fluorescence time course data was then analyzed using a custom Python script that performed subthreshold trace extraction and spike train generation. Briefly, the subthreshold activity was identified using asymmetric least squares regression and subtracted from raw time course data to generate a flattened trace containing a flat baseline and spiking activity. Spikes were identified from the flattened trace using a threshold of +6 STDEV of all cellular fluorescence values within a coverslip to generate a digitized spike train containing all-or-nothing firing data or Raster plot. Factor analysis was performed using the FactoryAnalyzer module with no rotation. The shared variance values per network were compared using Cohen's d.

Preparation of extracellular vesicles for mass spectrometry

Extracellular vesicles were enriched as described above in the section Isolation and labeling of extracellular vesicles. Enriched EVs were labeled with membrane-impermeable sulfo-NHS-biotin (Thermo Fisher Scientific, 21217) per the manufacturer's protocol. In brief, EVs in pH 8.0 PBS were labeled for 30 min at room temperature with sulfo-NHS-biotin (2 mM) and were quenched by the addition of 100 mM glycine. EVs solutions were desalted using spin columns. EVs were lysed by the subsequent addition of 10X RIPA buffer. Samples were prepared in triplicate, and triplicate control samples were treated equivalently, except sulfo-NHS-biotin was excluded. All samples were enriched using streptavidin magnetic beads (Pierce, #88817) and the DynaMag-2 Magnet (Invitrogen, #12321D) based on a protocol adopted from previous work.[44] Buffers were made fresh, including ETDA buffer (150 mM NaCl, 100 mM Tris pH 8, 0.5 mM EDTA pH 8), urea buffer (2 < urea, 10 mM Tris) and elution buffer (5% SDS in RIPA, 20 mM DTT, 2 mM biotin). 25 µL of streptavidin beads were used per sample, and beads were washed with 50 µL of cold RIPA twice before being resuspended in 25 µL cold RIPA. Beads were added to each sample, which were continuously rotated overnight at 4 C. The next day, the unbound fraction was removed from the beads and kept. Beads were washed with 100 µL RIPA, which was added to the saved unbound fraction (labeled FT, flow through) for each sample. Next, beads were washed twice with 200 µL RIPA, three times with EDTA buffer, three times with 1.5 M NaCl, three times with

0.1 M NaHCO3, and once with urea buffer. Proteins were eluted from the beads by boiling at 95 C with 60 µL elution buffer for 10 min. The elution step was repeated, for a total of two elution steps, and elutes from each step were combined for a given sample. Digestion was performed for eluted and FT proteins using a micro S-trap protocol provided by the manufacturer (Protifi).[45] For FT samples, proteins were brought to 5% SDS and reduced with 10 mM DTT for 10 minutes at 95 C. Cysteines were alkylated using 40 mM iodoacetamide for 45 minutes each at room temperature in the dark. The lysate was then acidified with phosphoric acid, brought to approximately 80-90% methanol with 100 mM TEAB in 90% methanol, and loaded onto the S-trap column. Following washing with 100 mM TEAB in 90% methanol, trypsin (Promega) was added to the S-trap at a 20:1 protein:protease ratio for 90 minutes at 47 °C. Peptides were eluted in three steps that were collected in the same tube for a given sample: 40 µL of 50 mM TEAB, 40 µL 0.2% FA in water, and 40 µL of 0.2% FA in 50% ACN, all spun at 4,000 x g for 1 minute. Eluted peptides were dried via lyophilization.

Preparation of cell-surface labeled neurons for mass spectrometry

Samples were prepared following published cell surface capture protocols that label cell surface proteins through sialic acids.[46,47] and lysate protein concentrations were quantitated by BCA (Pierce). Lysates were digested using a mini S-trap protocol (Protifi), which is similar to the micro S-trap protocol above, but with different volumes. Lysates were brought to 5% SDS and reduced with 5 mM DTT for 5 minutes at 95 C. Cysteines were alkylated using 25 mM iodoacetamide for 45 minutes each at room temperature in the dark. Lysates were then acidified with phosphoric acid, brought to approximately 80-90% methanol with 100 mM TEAB in 90% methanol, and loaded onto the S-trap column. Following washing with 100 mM TEAB in 90% methanol, trypsin (Promega) was added to the S-trap at a 20:1 protein:protease ratio for 90 minutes at 47 °C. Peptides were eluted in three steps that were collected in the same tube for a given sample: 80 µL of 50 mM TEAB, 80 µL 0.2% FA in water, and 80 µL of 0.2% FA in 50% ACN, all spun at 4,000 x g for 1 minute. Eluted peptides were dried via lyophilization and dried peptides were then resuspended in 100 µL 100 mM Tris, pH 8 for enrichment via streptavidin beads (Pierce, #88817) and the DynaMag-2 Magnet (Invitrogen, #12321D). Buffers were made fresh, including ETDA buffer (150 mM NaCl, 100 mM Tris pH 8, 0.5 mM EDTA pH 8). 50 µL of streptavidin beads were used per sample, and beads were washed with 200 µL 100 mM Tris three times before being resuspended in 400 µL 100 mM Tris. Beads were added to each sample (500 µL total per sample), which were continuously rotated overnight at 4 C. The next day, the unbound fraction was removed from the beads and kept. Beads were washed with 500 µL 100 mM Tris, which was added to the saved unbound fraction (labeled FT, flow through) for each sample. Next, beads were washed five times with 500 µL 100 mM Tris, five times with 500 µL EDTA buffer, five times with500 µL 1.5 M NaCl, five times with 500 µL 0.1 M NaHCO3, once with 500 µL 80% (v/v) 2-isopropanol, twice with500 µL water, and three times with 500 µL warm (60 °C) 100 mM Tris. Beads were then resuspended in 500 µL 100 mM Tris. Glycerol-free PNGaseF (New England Biolabs, # P0705L) was diluted 2-fold, and 1 µL of diluted PNGaseF was added to each set of beads. Beads with PNGaseF were incubated overnight, where PNGaseF enzymatic cleavgage release formerly N-glycosylated peptides (i.e., de-glycopeptides). Eluted de-glycopeptides were acidified with 10% FA before desalting with Strata-X reversed phase SPE cartridges (Phenomenex, #8B-S100-AAK) by conditioning the cartridge with 1 mL ACN followed by 1 mL 0.2% formic acid (FA) in water. Acidified de-glycopeptides loaded on to the cartridge, followed by a 1 mL wash with 0.2% FA in water. Peptides were eluted with 400 µL of 0.2% FA in 80% ACN and dried via lyophilization.

Mass spectrometry proteomics LC-MS/MS

All samples were resuspended in 0.2% formic acid in water prior to LC-MS/MS analysis, where half of the sample was injected for analysis (i.e., 5 µL or 10 µL total), and non-modified peptides and de-glycopeptides (referred to collectively as peptides in this section) were analyzed with the same LC-MS/MS method. All peptide mixtures were separated over a 25 cm EasySpray reversed phase LC column (75 µm inner diameter packed with 2 µm, 100 Å, PepMap C18 particles, Thermo Fisher Scientific). The mobile phases (A: water with

0.2% formic acid and B: acetonitrile with 0.2% formic acid) were driven and controlled by a Dionex µLtimate 3000 RPLC nano system (Thermo Fisher Scientific). An integrated loading pump was used to load peptides onto a trap column (Acclaim PepMap 100 C18, 5 um particles, 20 mm length, Thermo Fisher Scientific) at 5 µL/min, which was put in line with the analytical column 5.5 minutes into the gradient. The gradient increased from 0% to 5% B between 6 and 6.5 minutes, followed by an increase from 5% to 22% B from 6.5 to 66.5 minutes, an increase from 22% to 90% B from 66.5 to 71 minutes, isocratic flow at 90% B from 71 to 75 minutes, and a re-equilibration at 0% B for 15 minutes for a total analysis time of 90 minutes per injection. Eluted peptides were analyzed on an Orbitrap Fusion Tribrid MS system (Thermo Fisher Scientific). Precursors were ionized using an EASY-Spray ionization source (Thermo Fisher Scientific) source held at +2.2 kV compared to ground, and the column was held at 40 °C. The inlet capillary temperature was held at 275 °C. Survey scans of peptide precursors were collected in the Orbitrap from 350-1350 Th with an AGC target of 1,000,000, a maximum injection time of 50 ms, and a resolution of 60,000 at 200 m/z. Monoisotopic precursor selection was enabled for peptide isotopic distributions, precursors of z = 2-5 were selected for data-dependent MS/MS scans for 2 second of cycle time, and dynamic exclusion was set to 30 seconds with a ±10 ppm window set around the precursor monoisotope. An isolation window of 1 Th was used to select precursor ions with the quadrupole. MS/MS scans were collected using HCD at 30 normalized collision energy (nce) with an AGC target of 100,000 (200%) and a maximum injection time of 54 ms. Mass analysis was performed in the Orbitrap with a resolution of 30,000 with a first mass set at 120 Th.

Proteomics data analysis

Peptides from EV labeled data were searched with Morhpeus search algorithm[48] housed in the MetaMorpheus software environment (version 0.0.312)[49] using the entire mouse proteome downloaded from Uniprot[50] (reviewed, 17030 entries). Cleavage specificity was set to fully tryptic with 2 missed cleavage allowed and a minimum length of 7 residues, oxidation of methionine was set as a variable modification, and carbamidomethylation of cysteine was set as a fixed modification. Precursor and product ion tolerances were set to 5 ppm and 20 ppm, respectively. Output was set to filter at a q-value of 0.01, and FlashLFQ[51] with matching between runs was enabled. All other parameters were set as default. For quantitative comparisons, protein intensity values were log2 transformed prior to further analysis, proteins with greater than three missing values (i.e., half) per condition were removed, and missing values were imputed from a normal distribution with width 0.3 and downshift value of 1.8 (i.e., default values) using the Perseus software suite[6]. De-glycopeptides were searched with the Andromeda search engine[52] in MaxQuant.[53] Cleavage specificity was set to fully tryptic with 2 missed cleavage allowed and a minimum length of 7 residues, oxidation of methionine and deamidation of asparagine were set as a variable modification, and carbamidomethylation of cysteine was set as a fixed modification. Defaults were used for the remaining settings, including PSM and protein FDR thresholds of 0.01; and 20 ppm, 4.5 ppm, and 20 ppm for first search MS1 tolerance, main search MS1 tolerance, and MS2 product ion tolerance, respectively. The Deamidation Sites table was used for further data analysis, randomly chosen spectra were spot-checked for identification accuracy using IPSA to ensure data quality, and deamidated peptides were marked as either “True” or “False” for whether they contained the N-glycosylation sequon, N-X-S/T, where X is any residue but proline. This Deamidation Sites table file was then uploaded into Perseus and further filtered to remove 1) potential contaminants and reverse hits, 2) peptides that did not contain the N-glycosylation sequon, 3) sites with less than 0.5 localization probability, and 4) identifications that had more than three missing values. Missing values for the remaining identifications were imputed from a normal distribution with width 0.3 and downshift value of 1.8 (i.e., default values).

Statistical analysis

All statistical hypothesis tests were performed using either a hierarchical permutation test[54] (20,000 resamples for n=3 treatments, 70,000 for n=4, 200,000 for n>4) or a Welch’s t-test. Code is available at github.com/rishi-kulkarni/hierarch.

DNA oligonucleotides

Usage	DNA Sequence
mNeu3 KO sgRNA (FWD)	CACCGGAGAGGTGCCAGATTGTGTG
mNeu3 KO sgRNA (REV)	AAACCACACAATCTGGCACCTCTCC
murine safe-targeting sgRNA (FWD)	CACCGGAAATCCTTACCTAAGACAA
murine safe-targeting sgRNA (REV)	AAACTTGTCTTAGGTAAGGATTTCC
mNeu3 KO PCR (FWD)	GGGCCTTCAAGATTCTGTCCATTT
mNeu3 KO PCR (REV)	GTGCCATGTGACTCCAAAGTCATC
mNeu3 KO SEQ	TTTCAATGTCCTATATTGTTTGAAAAAAGAACTG
mNeu3 HDR sgRNA (FWD)	CACCGCGACTAAAGCCAAATCAAGA
mNeu3 HDR sgRNA (REV)	AAACTCTTGATTTGGCTTTAGTCGC
mNeu3 HDR PCR (FWD)	TCCCCGACCTGCAGCCCAGCT
mNeu3 HDR PCR (REV)	TGGAGAGGACTTTCCAAG
GAPDH qPCR (FWD)	CCCATCACCATCTTCCAGGAGC
GAPDH qPCR (REV)	CCAGTGAGCTTCCCGTTCAGC
mNEU1 qPCR (FWD)	TTCATCGCCATGAGGAGGTCCA
mNEU1 qPCR (REV)	AAAGGGAATGCCGCTCACTCCA
mNEU3 qPCR (FWD)	CTCAGTCAGAGATGAGGATGCT
mNEU3 qPCR (REV)	GTGAGACATAGTAGGCATAGGC
mNEU4 qPCR (FWD)	AGGAGAACGGTGCTCTTCCAGA
mNEU4 qPCR (REV)	GTTCTTGCCAGTGGCGATTTGC

DNA gene sequences and gBlocks

Gene	DNA Sequence
NEU3 HOM1	TCCCCGACCTGCAGCCCAGCTCTACACTCGGGAAGGCTGATCATCCCC GCCTATGCCTACTATGTCTCACGTTGGTTTCTCTGCTTTGCGTGTTCAGTCAAG CCCCATTCCCTGATGATCTACAGTGATGACTTTGGAGTCACATGGCACCATGGC AAGTTCATTGAGCCCCAGGTGACAGGGGAGTGCCAAGTGGCCGAAGTGGCTG GGACGGCTGGTAACCCTGTGCTCTACTGCAGTGCCCGAACACCAAGCCGATTT CGAGCAGAGGCTTTTAGTACTGATAGTGGTGGCTGCTTTCAGAAGCCAACCCT GAACCCACAACTCCATGAGCCTCGAACCGGCTGCCAAGGTAGTGTAGTGAGCT TCCGGCCTTTGAAGATGCCAAATACCTATCAAGACTCAATTGGCAAAGGTGCTC CCGCTACTCAGAAGTGCCCTCTGCTGGACAGTCCTCTGGAGGTGGAGAAAGGA GCTGAAACACCATCAGCAACATGGCTCTTGTACTCACATCCAACTAGCAAGAGG AAGAGGATTAACCTAGGCATCTACTACAACCGGAACCCCTTGGAGGTGAACTG CTGGTCCCGCCCGTGGATCTTGAACCGTGGGCCCAGTGGCTACTCTGATCTGG CTGTTGTGGAAGAACAGGACTTGGTGGCGTGTTTGTTTGAGTGTGGGGAGAAG AATGAGTATGAGCGGATTGACTTCTGTCTGTTTTCAGACCATGAGGTCCTGAGC TGTGAAGACTGTACCAGCCCTAGTAGCGACGGGAGCGGAGGAGGTTCCGG
NEU3 HOM2	AGTTCTTCTGATTCGAACATCGATGAGTGAGGCCCAGCTTCCCACAGAA AGGAATGGCAGCTACAGCCAGGGTAACAGAGGTCTCTGATGTCTAGAGAAAAC TCTAAAAACTAATAATCTGCTCCTTGAATTTTTTCACTTTTCCCTTCAATGAGCAT GGTGAAAATTGTGCCATATCTTACATAACGAGGCTCTTGAACTGGGAGTTTGAA TCTCTTCTCTTCCCATTAAAAGGAGAGGCCATGTGCTCGCTTCGCGTTCGACAA AGCCTGGATTCTGATCTTGAGTGGAAGCCACAGGCTTGTCTTTTCCAATGGTTC

	ACTGCTCACCTGAGTATTAGGTGATGTGTAGGTGCCTTGGCCAGAAGAAAGAT CTGTGTTGTTGTATTTTTTTAAATTTATTTATTTACTATATGTAAGTACACTGCAG CTGTCTTCAGACACACCAGAAGAGGGCGTCAGATCTCATTAGAGATGGTTGTG AGCCACCATGTGGTTGCTGGGATTTGAACTCAGGACCTTCAGAAGAGCAGTCA GTGCTCTTAACTACTGAGCCATCTCTCAAGCCCCGCATTGCTGTATTTTTAATAA GAAAAATGCCCTTATCCTTCCAATAATGCCTGGAGCTGTACAAATTCTCTGTCTT AGAAGACTTGAGAAAGCAGAACTGTAAGGTCAGATGCTTTCTCCAGCCTTGATG CTGTGTTCCACCTTCCCTTCCTCATCCAGAAAACAGTTACTAGGGAGAAAATGA GAAACCCATGCCAGCTGCCTTGGAAAGTCCTCTCCA
mNEU3 wt	ATGGAAGAGGTGCCTCCTTATAGCCTTAGTAGCACCCTGTTCCAGCAAG AAGAGCAGAGTGGAGTAACTTATAGAATCCCGGCTCTTCTCTATCTCCCCCCTA CGCATACATTTTTGGCATTTGCGGAAAAAAGGACATCCGTCCGGGATGAAGAT GCGGCGTGTCTCGTGTTGAGGAGAGGACTCATGAAAGGTCGCAGTGTTCAGTG GGGGCCACAGCGCCTCTTGATGGAAGCTACGCTTCCTGGGCACAGGACAATG AACCCGTGCCCGGTATGGGAAAAGAACACTGGAAGAGTTTACTTGTTCTTCATC TGCGTGAGGGGGCACGTCACAGAGCGGTGCCAGATAGTCTGGGGAAAGAATG CGGCGCGCCTTTGTTTTTTGTGCAGTGAAGATGCGGGATGCTCCTGGGGTGAG GTGAAGGATTTGACCGAAGAAGTCATTGGCTCTGAGGTGAAAAGATGGGCAAC CTTCGCTGTCGGACCAGGACACGGGATACAGCTGCATTCAGGCCGGCTGATCA TTCCGGCTTATGCCTACTATGTCTCCCGCTGGTTCCTTTGTTTTGCATGCAGCG TCAAACCGCACTCCCTCATGATATACTCCGACGATTTCGGGGTGACATGGCATC ACGGAAAGTTCATTGAACCTCAAGTCACCGGTGAATGCCAGGTCGCGGAGGTG GCAGGTACAGCCGGCAACCCGGTCCTTTATTGCAGCGCTCGGACCCCGTCCC GCTTTAGAGCCGAAGCCTTTAGTACAGATTCTGGCGGCTGCTTCCAAAAACCG ACTCTCAACCCTCAACTCCACGAACCTAGAACAGGTTGCCAAGGAAGCGTTGT GAGCTTCCGGCCGTTGAAGATGCCAAACACATATCAAGACTCTATCGGTAAGG GGGCGCCTGCGACGCAAAAGTGTCCACTCCTCGACAGCCCACTGGAGGTCGA GAAAGGCGCGGAAACCCCTTCCGCGACGTGGTTGCTGTATTCACATCCCACTA GCAAGAGGAAGAGAATTAACCTGGGGATTTACTACAATCGCAACCCGCTGGAG GTTAACTGCTGGAGTCGGCCGTGGATCCTTAACCGGGGTCCATCAGGCTACAG CGACCTGGCGGTAGTTGAGGAGCAGGATTTGGTGGCTTGCCTCTTTGAGTGCG GGGAGAAGAACGAATATGAGCGGATCGATTTCTGTTTGTTTTCTGATCACGAAG TATTGTCATGTGAAGATTGTACTTCCCCGTCTTCAGACGGGAGCGGAGGAGGT TCCGGtggaggtggttctggagattacaaggatgacgacgataagggcgattacaaggatgacgacgataagg gagattacaaggatgacgacgataag
mNEU3 Y369F	ATGGAAGAGGTGCCTCCTTATAGCCTTAGTAGCACCCTGTTCCAGCAAG AAGAGCAGAGTGGAGTAACTTATAGAATCCCGGCTCTTCTCTATCTCCCCCCTA CGCATACATTTTTGGCATTTGCGGAAAAAAGGACATCCGTCCGGGATGAAGAT GCGGCGTGTCTCGTGTTGAGGAGAGGACTCATGAAAGGTCGCAGTGTTCAGTG GGGGCCACAGCGCCTCTTGATGGAAGCTACGCTTCCTGGGCACAGGACAATG AACCCGTGCCCGGTATGGGAAAAGAACACTGGAAGAGTTTACTTGTTCTTCATC TGCGTGAGGGGGCACGTCACAGAGCGGTGCCAGATAGTCTGGGGAAAGAATG CGGCGCGCCTTTGTTTTTTGTGCAGTGAAGATGCGGGATGCTCCTGGGGTGAG GTGAAGGATTTGACCGAAGAAGTCATTGGCTCTGAGGTGAAAAGATGGGCAAC CTTCGCTGTCGGACCAGGACACGGGATACAGCTGCATTCAGGCCGGCTGATCA TTCCGGCTTATGCCTACTATGTCTCCCGCTGGTTCCTTTGTTTTGCATGCAGCG TCAAACCGCACTCCCTCATGATATACTCCGACGATTTCGGGGTGACATGGCATC ACGGAAAGTTCATTGAACCTCAAGTCACCGGTGAATGCCAGGTCGCGGAGGTG GCAGGTACAGCCGGCAACCCGGTCCTTTATTGCAGCGCTCGGACCCCGTCCC

	GCTTTAGAGCCGAAGCCTTTAGTACAGATTCTGGCGGCTGCTTCCAAAAACCG ACTCTCAACCCTCAACTCCACGAACCTAGAACAGGTTGCCAAGGAAGCGTTGT GAGCTTCCGGCCGTTGAAGATGCCAAACACATATCAAGACTCTATCGGTAAGG GGGCGCCTGCGACGCAAAAGTGTCCACTCCTCGACAGCCCACTGGAGGTCGA GAAAGGCGCGGAAACCCCTTCCGCGACGTGGTTGCTGTATTCACATCCCACTA GCAAGAGGAAGAGAATTAACCTGGGGATTTACTACAATCGCAACCCGCTGGAG GTTAACTGCTGGAGTCGGCCGTGGATCCTTAACCGGGGTCCATCAGGCTTTAG CGACCTGGCGGTAGTTGAGGAGCAGGATTTGGTGGCTTGCCTCTTTGAGTGCG GGGAGAAGAACGAATATGAGCGGATCGATTTCTGTTTGTTTTCTGATCACGAAG TATTGTCATGTGAAGATTGTACTTCCCCGTCTTCAGACGGGAGCGGAGGAGGT TCCGGtggaggtggttctggagattacaaggatgacgacgataagggcgattacaaggatgacgacgataagg gagattacaaggatgacgacgataag

75

References.

(1) Wu, Y.; Dissing-Olesen, L.; MacVicar, B. A.; Stevens, B. Microglia: Dynamic Mediators of Synapse Development and Plasticity. *Trends Immunol.* **2015**, *36* (10), 605–613. https://doi.org/10.1016/j.it.2015.08.008.

(2) Szepesi, Z.; Manouchehrian, O.; Bachiller, S.; Deierborg, T. Bidirectional Microglia–Neuron Communication in Health and Disease. *Front. Cell. Neurosci.* **2018**, *12* (September), 1–26. https://doi.org/10.3389/fncel.2018.00323.

(3) Cakir, B.; Kiral, F. R.; Park, I. H. Advanced in Vitro Models: Microglia in Action. *Neuron* **2022**, *110* (21), 3444–3457. https://doi.org/10.1016/j.neuron.2022.10.004.

(4) Paolicelli, R. C.; Sierra, A.; Stevens, B.; Tremblay, M. E.; Aguzzi, A.; Ajami, B.; Amit, I.; Audinat, E.; Bechmann, I.; Bennett, M.; et al. Microglia States and Nomenclature: A Field at Its Crossroads. *Neuron* **2022**, *110* (21), 3458–3483. https://doi.org/10.1016/j.neuron.2022.10.020.

(5) Stephan, A. H.; Barres, B. A.; Stevens, B. The Complement System: An Unexpected Role in Synaptic Pruning during Development and Disease. *Annu. Rev. Neurosci.* **2012**, *35*, 369–389. https://doi.org/10.1146/annurev-neuro-061010-113810.

(6) Zhang, J.; Malik, A.; Choi, H. B.; Ko, R. W. Y.; Dissing-Olesen, L.; MacVicar, B. A. Microglial CR3 Activation Triggers Long-Term Synaptic Depression in the Hippocampus via NADPH Oxidase. *Neuron* **2014**, *82* (1), 195–207. https://doi.org/10.1016/j.neuron.2014.01.043.

(7) Klaus, C.; Hansen, J. N.; Ginolhac, A.; Gérard, D.; Gnanapragassam, V. S.; Horstkorte, R.; Rossdam, C.; Buettner, F. F. R.; Sauter, T.; Sinkkonen, L.; et al. Reduced Sialylation Triggers Homeostatic Synapse and Neuronal Loss in Middle-Aged Mice. *Neurobiol. Aging* **2020**, *88*, 91–107. https://doi.org/10.1016/j.neurobiolaging.2020.01.008.

(8) Cunningham, C. Microglia and Neurodegeneration: The Role of Systemic Inflammation. *Glia* **2013**, *61* (1), 71–90. https://doi.org/10.1002/glia.22350.

(9) Palop, J. J.; Mucke, L. Synaptic Depression and Aberrant Excitatory Network Activity in Alzheimer's Disease: Two Faces of the Same Coin? *NeuroMolecular Med.* **2010**, *12* (1), 48–55. https://doi.org/10.1007/s12017-009-8097-7.

(10) Kulkarni, A. S.; Burns, M. R.; Brundin, P.; Wesson, D. W. Linking α-Synuclein-Induced Synaptopathy and Neural Network Dysfunction in Early Parkinson's Disease. *Brain Commun.* **2022**, *4* (4). https://doi.org/10.1093/braincomms/fcac165.

(11) Schedin-Weiss, S.; Winblad, B.; Tjernberg, L. O. The Role of Protein Glycosylation in Alzheimer Disease. *FEBS J.* **2014**, *281* (1), 46–62. https://doi.org/10.1111/febs.12590.

(12) Demina, E. P.; Pierre, W. C.; Nguyen, A. L. A.; Londono, I.; Reiz, B.; Zou, C.; Chakraberty, R.; Cairo, C. W.; Pshezhetsky, A. V.; Lodygensky, G. A. Persistent Reduction in Sialylation of Cerebral Glycoproteins Following Postnatal Inflammatory Exposure 11 Medical and Health Sciences 1109 Neurosciences. *J. Neuroinflammation* **2018**, *15* (1), 1–14. https://doi.org/10.1186/s12974-018-1367-2.

(13) Schnaar, R. L.; Gerardy-Schahn, R.; Hildebrandt, H. Sialic Acids in the Brain: Gangliosides and Polysialic Acid in Nervous System Development, Stability, Disease, and Regeneration. *Physiol. Rev.* **2014**, *94* (2), 461–518. https://doi.org/10.1152/physrev.00033.2013.

(14) Allendorf, D. H.; Franssen, E. H.; Brown, G. C. Lipopolysaccharide Activates Microglia via Neuraminidase 1 Desialylation of Toll-like Receptor 4. *J. Neurochem.* **2020**, *155* (4), 403–416. https://doi.org/10.1111/jnc.15024.

(15) Allendorf, D. H.; Brown, G. C. Neu1 Is Released From Activated Microglia, Stimulating Microglial Phagocytosis and Sensitizing Neurons to Glutamate. *Front. Cell. Neurosci.* **2022**, *16* (May), 1–13. https://doi.org/10.3389/fncel.2022.917884.

(16) Pluvinage, J. V.; Haney, M. S.; Smith, B. A. H.; Sun, J.; Iram, T.; Bonanno, L.; Li, L.; Lee, D. P.;

Morgens, D. W.; Yang, A. C.; et al. CD22 Blockade Restores Homeostatic Microglial Phagocytosis in Ageing Brains. *Nature* **2019**, *568* (7751), 187–192. https://doi.org/10.1038/s41586-019-1088-4.

(17) Nomura, K.; Vilalta, A.; Allendorf, D. H.; Hornik, T. C.; Brown, G. C. Activated Microglia Desialylate and Phagocytose Cells via Neuraminidase, Galectin-3, and Mer Tyrosine Kinase. *J. Immunol.* **2017**, 1502532. https://doi.org/10.4049/jimmunol.1502532.

(18) Linnartz, B.; Kopatz, J.; Tenner, A. J.; Neumann, H. Sialic Acid on the Neuronal Glycocalyx Prevents Complement C1 Binding and Complement Receptor-3-Mediated Removal by Microglia. *J. Neurosci.* **2012**, *32* (3), 946–952. https://doi.org/10.1523/JNEUROSCI.3830-11.2012.

(19) Ereño-Orbea, J.; Sicard, T.; Cui, H.; Mazhab-Jafari, M. T.; Benlekbir, S.; Guarné, A.; Rubinstein, J. L.; Julien, J. P. Molecular Basis of Human CD22 Function and Therapeutic Targeting. *Nat. Commun.* **2017**, *8* (1), 1–11. https://doi.org/10.1038/s41467-017-00836-6.

(20) Fernández-Arjona, M. D. M.; Grondona, J. M.; Fernández-Llebrez, P.; López-Ávalos, M. D. Microglial Activation by Microbial Neuraminidase through TLR2 and TLR4 Receptors. *J. Neuroinflammation* **2019**, *16* (1), 1–14. https://doi.org/10.1186/s12974-019-1643-9.

(21) Kulkarni, R. U.; Wang, C. L.; Bertozzi, C. R. Subthreshold Voltage Analysis Demonstrates Neuronal Cell-Surface Sialic Acids Modulate Excitability and Network Integration. *bioRxiv* **2020**, 2020.04.07.030866.

(22) Isaeva, E.; Lushnikova, I.; Savrasova, A.; Skibo, G.; Holmes, G. L.; Isaev, D. Blockade of Endogenous Neuraminidase Leads to an Increase of Neuronal Excitability and Activity-Dependent Synaptogenesis in the Rat Hippocampus. *Eur. J. Neurosci.* **2010**, *32* (11), 1889–1896. https://doi.org/10.1111/j.1460-9568.2010.07468.x.

(23) Allendorf, D. H.; Puigdellívol, M.; Brown, G. C. Activated Microglia Desialylate Their Surface, Stimulating Complement Receptor 3-Mediated Phagocytosis of Neurons. *Glia* **2020**, *68* (5), 989–998. https://doi.org/10.1002/glia.23757.

(24) Nomura, K.; Vilalta, A.; Allendorf, D. H.; Hornik, T. C.; Brown, G. C. Activated Microglia Desialylate and Phagocytose Cells via Neuraminidase, Galectin-3, and Mer Tyrosine Kinase. *J. Immunol.* **2017**, *198* (12), 4792–4801. https://doi.org/10.4049/jimmunol.1502532.

(25) Hata, K.; Koseki, K.; Yamaguchi, K.; Moriya, S.; Suzuki, Y.; Yingsakmongkon, S.; Hirai, G.; Sodeoka, M.; Von Itzstein, M.; Miyagi, T. Limited Inhibitory Effects of Oseltamivir and Zanamivir on Human Sialidases. *Antimicrob. Agents Chemother.* **2008**, *52* (10), 3484–3491. https://doi.org/10.1128/AAC.00344-08.

(26) Pshezhetsky, A. V.; Ashmarina, M. Keeping It Trim: Roles of Neuraminidases in CNS Function. *Glycoconj. J.* **2018**, *35* (4), 375–386. https://doi.org/10.1007/s10719-018-9837-4.

(27) Smutova, V.; Albohy, A.; Pan, X.; Korchagina, E.; Miyagi, T.; Bovin, N.; Cairo, C. W.; Pshezhetsky, A. V. Structural Basis for Substrate Specificity of Mammalian Neuraminidases. *PLoS One* **2014**, *9* (9), 1–11. https://doi.org/10.1371/journal.pone.0106320.

(28) Albohy, A.; Li, M. D.; Zheng, R. B.; Zou, C.; Cairo, C. W. Insight into Substrate Recognition and Catalysis by the Human Neuraminidase 3 (NEU3) through Molecular Modeling and Site-Directed Mutagenesis. *Glycobiology* **2010**, *20* (9), 1127–1138. https://doi.org/10.1093/glycob/cwq077.

(29) Sandbhor, M. S.; Soya, N.; Albohy, A.; Zheng, R. B.; Cartmell, J.; Bundle, D. R.; Klassen, J. S.; Cairo, C. W. Substrate Recognition of the Membrane-Associated Sialidase NEU3 Requires a Hydrophobic Aglycone. *Biochemistry* **2011**, *50* (32), 6753–6762. https://doi.org/10.1021/bi200449j.

(30) Albohy, A.; Richards, M. R.; Cairo, C. W. Mapping Substrate Interactions of the Human Membrane-Associated Neuraminidase, NEU3, Using STD NMR. *Glycobiology* **2014**, *25* (3), 284–293. https://doi.org/10.1093/glycob/cwu109.

(31) Zanchetti, G.; Colombi, P.; Manzoni, M.; Anastasia, L.; Caimi, L.; Borsani, G.; Venerando, B.; Tettamanti, G.; Preti, A.; Monti, E.; et al. Sialidase NEU3 Is a Peripheral Membrane Protein Localized on

the Cell Surface and in Endosomal Structures. *Biochem. J.* **2007**, *408* (2), 211–219. https://doi.org/10.1042/BJ20070503.

(32) Rodriguez-Walker, M.; Daniotti, J. L. Human Sialidase Neu3 Is S-Acylated and Behaves Like an Integral Membrane Protein. *Sci. Rep.* **2017**, *7* (1), 1–13. https://doi.org/10.1038/s41598-017-04488-w.

(33) Yang, Y.; Boza-Serrano, A.; Dunning, C. J. R.; Clausen, B. H.; Lambertsen, K. L.; Deierborg, T. Inflammation Leads to Distinct Populations of Extracellular Vesicles from Microglia. *J. Neuroinflammation* **2018**, *15* (1), 1–19. https://doi.org/10.1186/s12974-018-1204-7.

(34) Kumar, D.; Gupta, D.; Shankar, S.; Srivastava, R. K. Biomolecular Characterization of Exosomes Released from Cancer Stem Cells: Possible Implications for Biomarker and Treatment of Cancer. *Oncotarget* **2015**, *6* (5), 3280–3291. https://doi.org/10.18632/oncotarget.2462.

(35) Kosaka, N.; Iguchi, H.; Yoshioka, Y.; Takeshita, F.; Matsuki, Y.; Ochiya, T. Secretory Mechanisms and Intercellular Transfer of MicroRNAs in Living Cells. *J. Biol. Chem.* **2010**, *285* (23), 17442–17452. https://doi.org/10.1074/jbc.M110.107821.

(36) Huang, Y. L.; Walker, A. S.; Miller, E. W. A Photostable Silicon Rhodamine Platform for Optical Voltage Sensing. *J. Am. Chem. Soc.* **2015**, *137* (33), 10767–10776. https://doi.org/10.1021/jacs.5b06644.

(37) Paolini, L.; Orizio, F.; Busatto, S.; Radeghieri, A.; Bresciani, R.; Bergese, P.; Monti, E. Exosomes Secreted by Hela Cells Shuttle on Their Surface the Plasma Membrane-Associated Sialidase NEU3. *Biochemistry* **2017**, *56* (48), 6401–6408. https://doi.org/10.1021/acs.biochem.7b00665.

(38) Klenk, E. Neuraminsäure, Das Spaltprodukt Eines Neuen Gehirnlipoids. *Hoppe. Seylers. Z. Physiol. Chem.* **1941**, *268* (1–2), 50–58. https://doi.org/10.1515/bchm2.1941.268.1-2.50.

(39) Sanjana, N. E.; Shalem, O.; Zhang, F. Improved Vectors and Genome-Wide Libraries for CRISPR Screening IPipet□: Sample Handling Using a Tablet. *Nat. Publ. Gr.* **2014**, *11* (8), 783–784. https://doi.org/10.1038/nmeth.3047.

(40) Haney, M. S.; Bohlen, C. J.; Morgens, D. W.; Ousey, J. A.; Barkal, A. A.; Tsui, C. K.; Ego, B. K.; Levin, R.; Kamber, R. A.; Collins, H.; et al. Identification of Phagocytosis Regulators Using Magnetic Genome-Wide CRISPR Screens. *Nat. Genet.* **2018**, *50* (12), 1716–1727. https://doi.org/10.1038/s41588-018-0254-1.

(41) Pronobis, M. I.; Deuitch, N.; Peifer, M. The Miraprep□: A Protocol That Uses a Miniprep Kit and Provides Maxiprep Yields. **2016**, No. Table 1, 1–12. https://doi.org/10.1371/journal.pone.0160509.

(42) Brinkman, E. K.; van Steensel, B. Rapid Quantitative Evaluation of CRISPR Genome Editing by TIDE and TIDER. In *CRISPR Gene Editing: Methods and Protocols*; 2019; pp 29–44.

(43) Savic, D.; Partridge, E. C.; Newberry, K. M.; Smith, S. B.; Meadows, S. K.; Roberts, B. S.; Mackiewicz, M.; Mendenhall, E. M.; Myers, R. M. CETCh-Seq□: CRISPR Epitope Tagging ChIP-Seq of DNA-Binding Proteins. *Genome Res.* **2015**, 1581–1589. https://doi.org/10.1101/gr.193540.115.

(44) Wei, W.; Riley, N. M.; Yang, A. C.; Kim, J. T.; Terrell, S. M.; Li, V. L.; Garcia-Contreras, M.; Bertozzi, C. R.; Long, J. Z. Cell Type-Selective Secretome Profiling in Vivo. *Nat. Chem. Biol.* **2021**, *17* (3), 326–334. https://doi.org/10.1038/s41589-020-00698-y.

(45) HaileMariam, M.; Eguez, R. V.; Singh, H.; Bekele, S.; Ameni, G.; Pieper, R.; Yu, Y. S-Trap, an Ultrafast Sample-Preparation Approach for Shotgun Proteomics. *J. Proteome Res.* **2018**, *17* (9), 2917–2924. https://doi.org/10.1021/acs.jproteome.8b00505.

(46) Bausch-Fluck, D.; Hofmann, A.; Bock, T.; Frei, A. P.; Cerciello, F.; Jacobs, A.; Moest, H.; Omasits, U.; Gundry, R. L.; Yoon, C.; et al. A Mass Spectrometric-Derived Cell Surface Protein Atlas. *PLoS One* **2015**, *10* (4), 1–22. https://doi.org/10.1371/journal.pone.0121314.

(47) Leung, K. K.; Wilson, G. M.; Kirkemo, L. L.; Riley, N. M.; Coon, J. J.; Wells, J. A. Broad and Thematic Remodeling of the Surfaceome and Glycoproteome on Isogenic Cells Transformed with Driving Proliferative Oncogenes. *Proc. Natl. Acad. Sci. U. S. A.* **2020**, *117* (14), 7764–7775.

https://doi.org/10.1073/pnas.1917947117.

(48) Wenger, C. D.; Coon, J. J. A Proteomics Search Algorithm Specifically Designed for High-Resolution Tandem Mass Spectra. *J. Proteome Res.* **2013**, *12* (3), 1377–1386. https://doi.org/10.1021/pr301024c.

(49) Solntsev, S. K.; Shortreed, M. R.; Frey, B. L.; Smith, L. M. Enhanced Global Post-Translational Modification Discovery with MetaMorpheus. *J. Proteome Res.* **2018**, *17* (5), 1844–1851. https://doi.org/10.1021/acs.jproteome.7b00873.

(50) Bateman, A. UniProt: A Worldwide Hub of Protein Knowledge. *Nucleic Acids Res.* **2019**, *47* (D1), D506–D515. https://doi.org/10.1093/nar/gky1049.

(51) Millikin, R. J.; Solntsev, S. K.; Shortreed, M. R.; Smith, L. M. Ultrafast Peptide Label-Free Quantification with FlashLFQ. *J. Proteome Res.* **2018**, *17* (1), 386–391. https://doi.org/10.1021/acs.jproteome.7b00608.

(52) Cox, J.; Neuhauser, N.; Michalski, A.; Scheltema, R. A.; Olsen, J. V; Mann, M. Andromeda: A Peptide Search Engine Integrated into the MaxQuant Environment. *J. Proteome Res.* **2011**, *10* (4), 1794–1805. https://doi.org/10.1021/pr101065j.

(53) Tyanova, S.; Temu, T.; Cox, J. The MaxQuant Computational Platform for Mass Spectrometry-Based Shotgun Proteomics. *Nat. Protoc.* **2016**, *11* (12), 2301–2319. https://doi.org/10.1038/nprot.2016.136.

(54) Kulkarni, R. U.; Wang, C. L.; Bertozzi, C. R. Analyzing Nested Experimental Designs—A User-Friendly Resampling Method to Determine Experimental Significance. *PLoS Comput. Biol.* **2022**, *18* (5), 1–26. https://doi.org/10.1371/journal.pcbi.1010061.

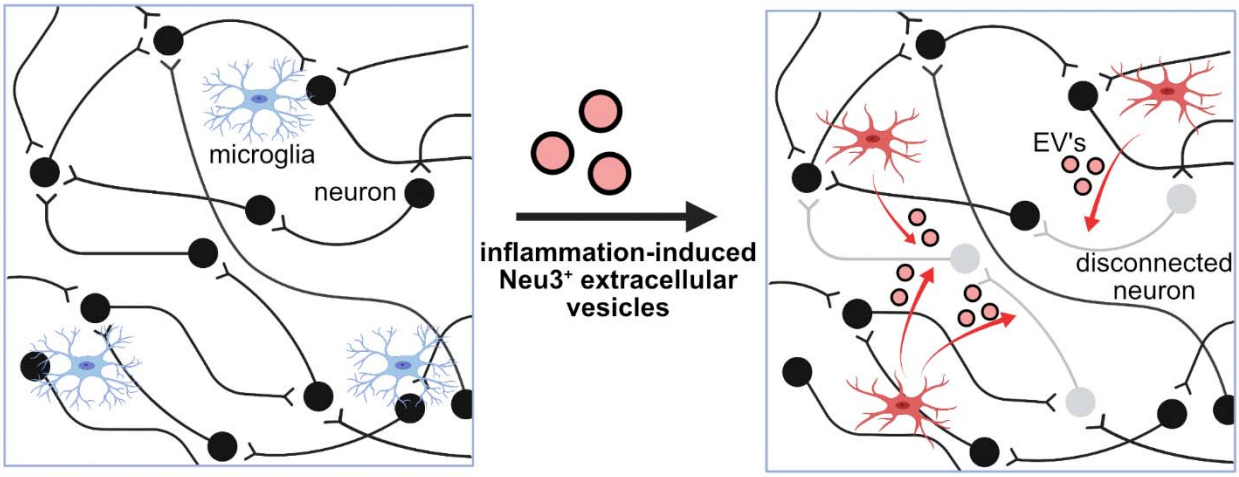

Graphical Abstract. Neuroinflammation induces secretion of the sialidase Neu3 via extracellular vesicles from microglia that prune neuronal synapses and disrupt neuronal communication.

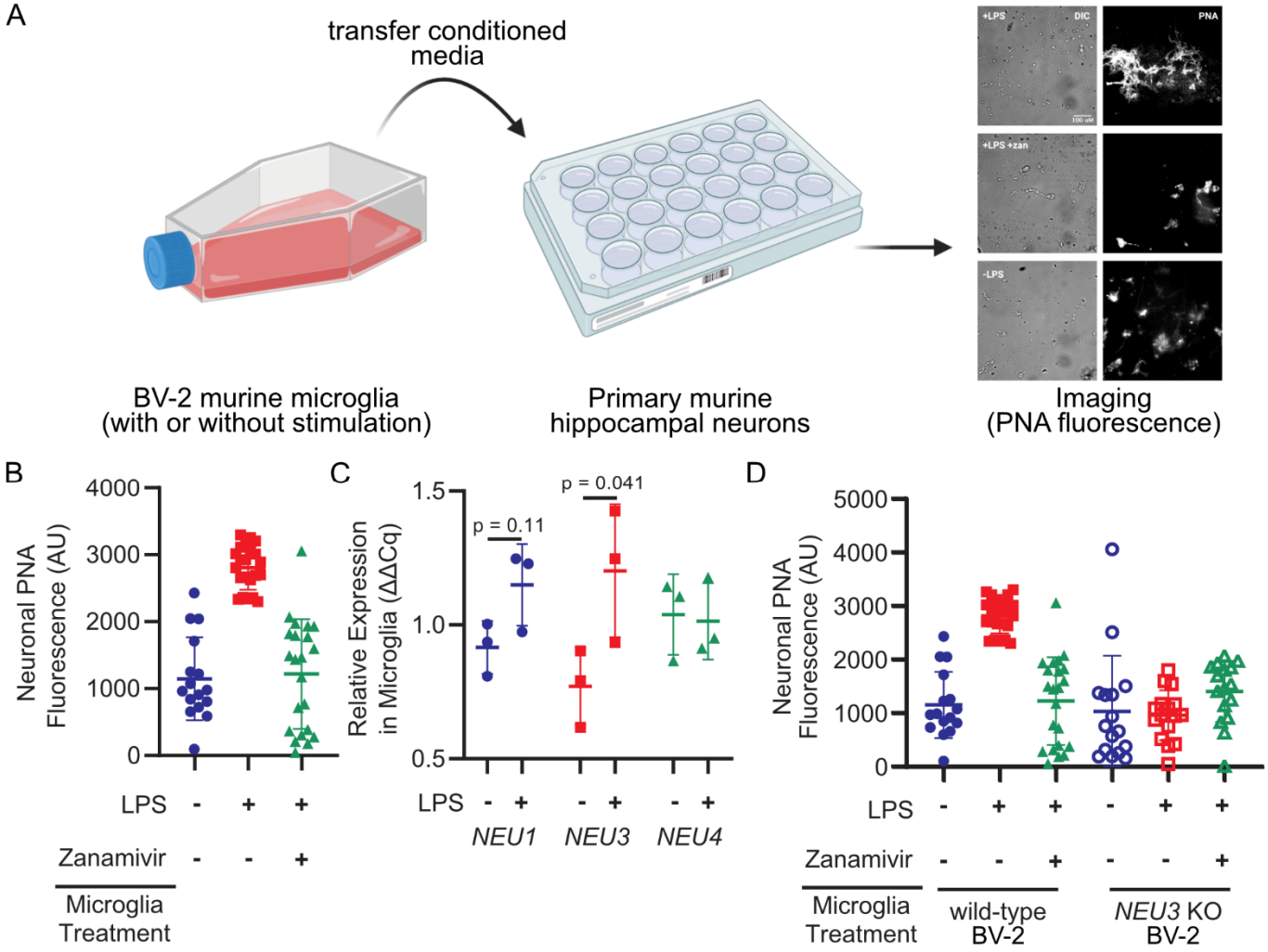

Figure 1. Microglia upregulate and NEU3 and active Neu3 is necessary for secreted sialidase activity. **(A, B)** Primary mouse hippocampal neurons were treated with conditioned media from resting or LPS-activated BV-2 microglia in the presence or absence of zanamivir. Representative scheme and images **(A)** and quantification of fluorescence **(B)** reveal that LPS-activation causes 3-fold increase in PNA signal compared to

resting (+LPS vs. -LPS, p=0.045), an effect abrogated by pharmacological sialidase inhibition (-LPS vs. +LPS +zan, p=0.90; +LPS vs. +LPS +zan, p=0.042). Hypothesis testing performed with hierarchical permutation test, n=3 coverslips/condition, avg. 20 neurons/condition. **(C)** Quantification of transcript levels of *NEU1*, *NEU3*, and *NEU4* by qPCR in resting and LPS-activated BV-2 microglia (*NEU1*, p=0.11; *NEU3*, p=0.041; *NEU4*, p=0.90). **(D)** Neurons were treated with conditioned media from wild-type (WT) or *NEU3* knockout (*NEU3* KO) BV-2 microglia, with or without deoxy-2,3-anhydroneuraminic acid (DANA), and stained with peanut agglutinin (PNA). Media from activated WT microglia produced a 3-fold increase in desialylation compared to resting (-LPS vs. +LPS, p=0.043; +LPS vs. +LPS+zan, p=0.042) but media from *NEU3* KO microglia exhibited no significant change in desialylation in response to LPS or zanamivir (-LPS vs. +LPS, p=0.74; +LPS vs. +LPS+zan, p=0.12). n=3 coverslips/condition, 60 total WT cells, 48 total *NEU3* KO cells. Hypothesis tests performed with hierarchical permutation test.

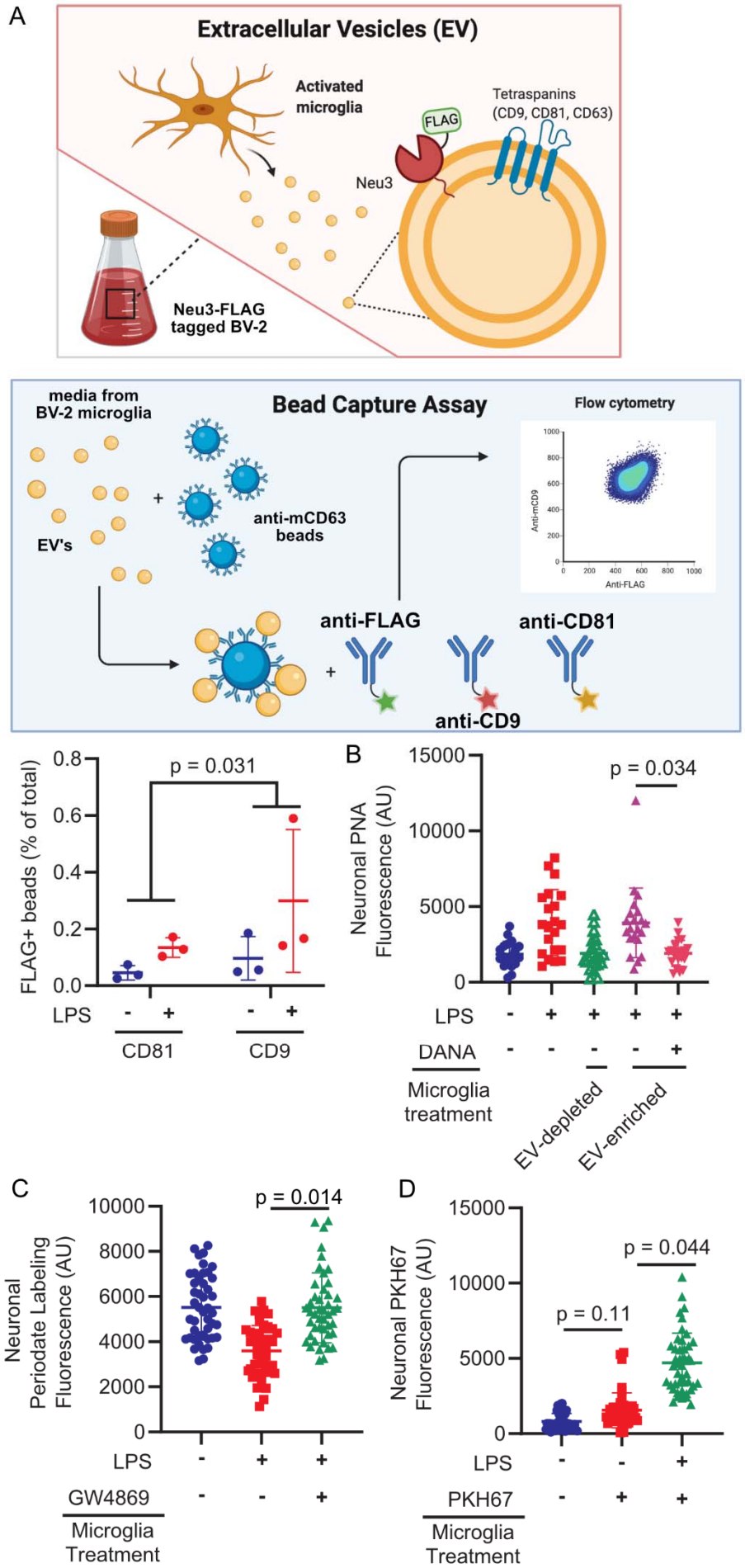
A
Extracellular Vesicles (EV)
Activated microglia
Tetraspanins (CD9, CD81, CD63)
FLAG
Neu3
Neu3-FLAG tagged BV-2
media from BV-2 microglia
Bead Capture Assay
Flow cytometry
EV's
anti-mCD63 beads
Anti-mCD9
Anti-FLAG
anti-FLAG
anti-CD81
anti-CD9
FLAG+ beads (% of total)
p = 0.031
LPS
CD81
CD9
B
Neuronal PNA Fluorescence (AU)
p = 0.034
LPS
DANA
Microglia treatment
EV-depleted
EV-enriched
C
Neuronal Periodate Labeling Fluorescence (AU)
p = 0.014
LPS
GW4869
Microglia Treatment
D
Neuronal PKH67 Fluorescence (AU)
p = 0.044
p = 0.11
LPS
PKH67
Microglia Treatment

Figure 2. Neu3 is associated with microglia-derived fusogenic extracellular vesicles. (A) Endogenous NEU3 was FLAG-tagged in BV-2 microglia by homology-directed recombination. After exposure of BV-2 microglia with endogenously FLAG-tagged Neu3 to vehicle or LPS, EVs were captured on anti-mCD81 or anti-mCD9 coupled beads, labeled with fluorophore-coupled anti-FLAG or anti-mCD63, and analyzed by flow cytometry. Bead captured-EV's demonstrate increased FLAG signal in LPS-treated microglia compared to resting microglia, indicating that *NEU3* colocalizes with EV markers and is released via EVs upon LPS-activation. (-LPS vs. +LPS, p-value = 0.031). n=3 wells/condition, 2 capture methods/well. **(B)** PNA staining of neuronal surfaces treated with EV-enriched or EV-depleted media of activated WT microglia reveals that EV-enriched fraction alone has sialidase activity (EV-enriched vs. EV-depleted, p=0.023; EV-enriched vs. EV-enriched+DANA, p=0.034). n=4 coverslips/condition, 7 cells/coverslip. **(C)** Periodate labeling of neuronal surface sialic acids reveals that pharmacologic inhibition of EV production with GW4869 abrogates sialidase activity of EV-enriched microglia media (-LPS vs. +LPS, p=0.027; -LPS vs. +LPS+GW4869, p=0.97; +LPS vs. +LPS+GW4869, p=0.014). n=3 coverslips/condition, 135 cells total. **(D)** Imaging of neurons treated with PKH67-stained microglial exosome demonstrates transferal of dye from EVs to neuronal membranes (Vehicle vs. -LPS, p=0.15; -LPS vs. +LPS, p=0.044). Hypothesis testing for all panels was performed using hierarchical permutation test. n=3 coverslips/condition, 15 cells/coverslip.

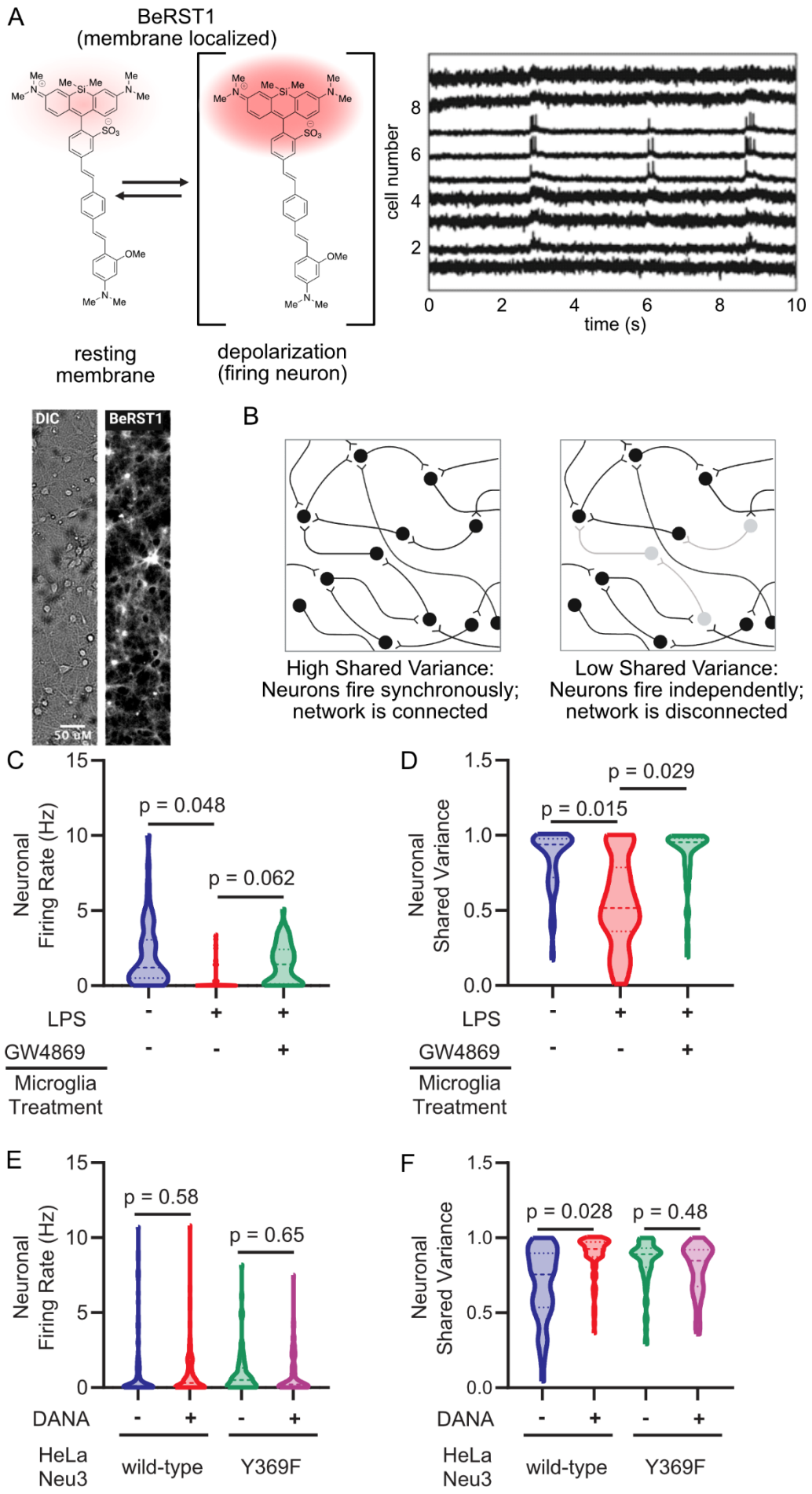
A
BeRST1
(membrane localized)
resting
membrane
depolarization
(firing neuron)
cell number
time (s)
DIC
BeRST1
50 uM
B
High Shared Variance:
Neurons fire synchronously;
network is connected
Low Shared Variance:
Neurons fire independently;
network is disconnected
C
Neuronal
Firing Rate (Hz)
p = 0.048
p = 0.062
LPS
GW4869
Microglia
Treatment
D
Neuronal
Shared Variance
p = 0.015
p = 0.029
LPS
GW4869
Microglia
Treatment
E
Neuronal
Firing Rate (Hz)
p = 0.58
p = 0.65
DANA
HeLa
Neu3
wild-type
Y369F
F
Neuronal
Shared Variance
p = 0.028
p = 0.48
DANA
HeLa
Neu3
wild-type
Y369F

Figure 3. Neu3 is necessary and sufficient to disrupt neuronal network connectivity. Neurons were labeled with the voltage-sensitive dye BeRST1 and treated with extracellular-vesicle enriched media from either microglia or Neu3 over-expressing cells. Neuronal firing rates and network connectivity were analyzed by fluorescence microscopy. **(A)** BeRST1 is a membrane-localizing voltage-sensitive fluorophore that undergoes a dramatic increase in fluorescence intensity in response to changes in membrane potential, i.e. upon the depolarization of firing neurons. Representative brightfield and BeRST1 fluorescence of a single field of view and voltage traces of each neuron in a single field of view contain both subthreshold activity and spiking activity. **(B)** Network connectivity is quantitated by measuring the spike traces for individual neurons within a single field of view, and then looking at the synchronicity of firing by the metric of Shared Variance. **(C,D)** BV-2 microglia treated with or without LPS and with or without GW4869. The EVs from the conditioned media were enriched and neurons were treated with EV-enriched media, and neuronal activity was measured by voltage imaging with BeRST1. **(C)** Firing rates of neurons treated with BV-2 EV-enriched media reveal 1.7 Hz decrease in +LPS condition compared to -LPS condition (p=0.048). The effect is partially rescued by inhibition of EV production with GW4869 (+LPS vs. +LPS+GW4869, p=0.062). (**D)** Treatment with EV-enriched media results in a 29% reduction in subthreshold shared variance per neuron in -LPS vs. +LPS conditions, suggesting that neurons are no longer well-connected to the network (p=0.015). Effect is rescued by addition of GW4869 (+LPS vs. +LPS+GW4869, p=0.029). **(E,F)** As in **(C,D)**, but using conditioned media from HeLa cells overexpressing either wild-type or loss-of-function (Y369F) Neu3. **(E)** Firing rates of neurons treated with EV-enriched media of NEU3-overexpressing HeLa cells reveal no significant changes between functional NEU3 and a loss-of-function point mutant (WT: -0.26 Hz, p=0.58; Y369F: -0.14 Hz, p=0.65). **(F)** Treatment with EV-enriched HeLa media reveals 15% reduction in subthreshold shared variance between WT and Y369F mutant (p=0.046). Coincubation of WT EV-enriched media with DANA prevents this reduction (p=0.028), while coincubation of Y369F media with DANA has no significant effect (p=0.48). For **(C,D)**: n=4 coverslips/condition, 168 neurons total. For **(E,F)**: n=3 coverslips/condition, 331 total neurons. All hypothesis testing was performed by hierarchical permutation tests.

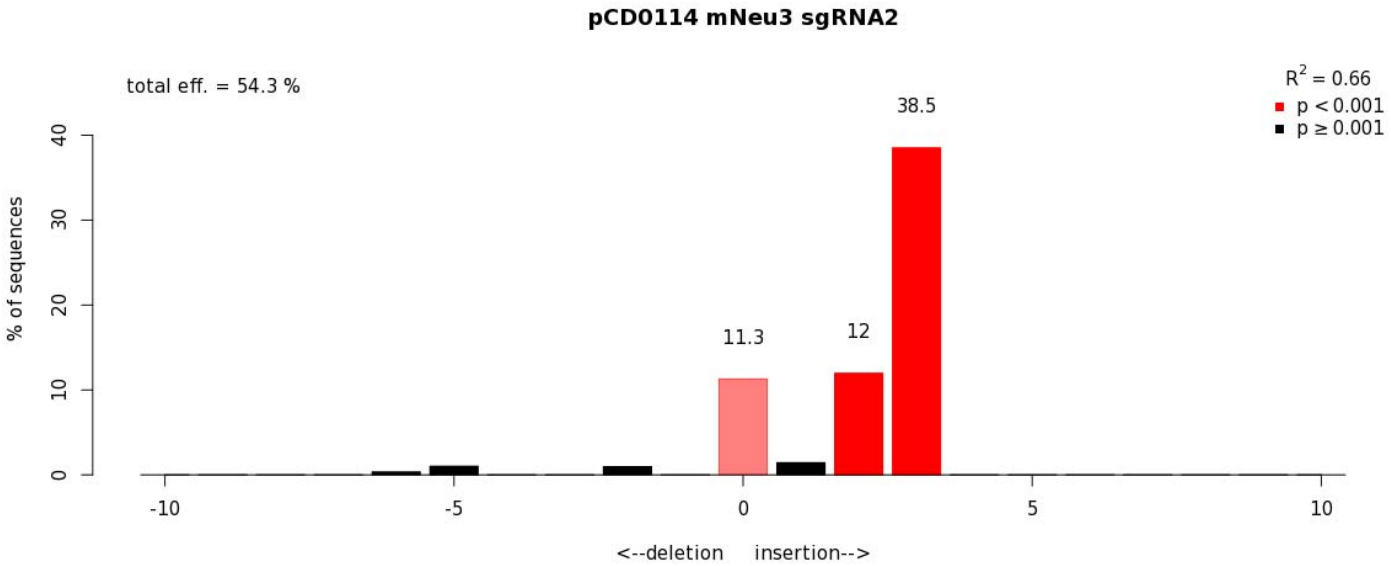

Figure S1. Tracking of Indels by Decomposition (TIDE) analysis of *NEU3* KO BV-2 microglia. To confirm knock-out of the *NEU3* gene in murine BV-2 microglia, CRISPR-Cas9 edited cells were subjected to two weeks of selection before genomic DNA was harvested and the cut region was amplified and sequenced. TIDE [ref] deconvolutes the possible changes from CRISPR-based editing to provide gene-level editing quantiation.

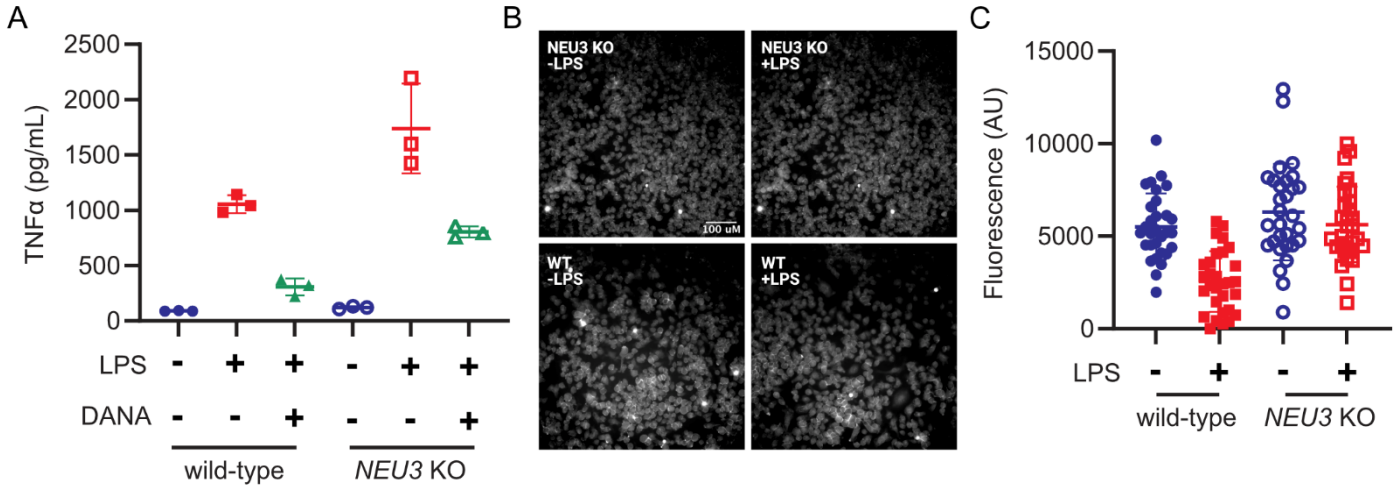

Figure S2. Neu3 desialylates microglia in cis but is not necessary for inflammatory activity. (A,B) Wild-type or *NEU3* knock-out (*NEU3* KO) BV-2 microglia were stimulated with LPS for 24 h, with or without deoxy-2,3-anhydroneuraminic acid (DANA). **(A)** Quantification of TNF-□ secretion by LPS-treated WT and NEU3 KO microglia by flow cytometry reveals that NEU3 KO microglia are capable of activating in response to LPS (WT: -LPS vs. +LPS, p=0.002; -LPS vs. +LPS+DANA, p=0.039; +LPS vs. +LPS+DANA, p=0.0003) (NEU3 KO: -LPS vs. +LPS, p=0.02; -LPS vs. +LPS+DANA, p=0.001; +LPS vs. +LPS+DANA, p=0.055). n=3 wells/condition. Hypothesis tests performed with Welch's t-test. **(B, C)** Periodate labeling of activated vs. resting WT and NEU3 KO microglia (WT, p=0.0383; NEU3 KO, p=0.5073). n=3 wells/condition, 10 microglia/well. All hypothesis tests performed with hierarchical permutation test.

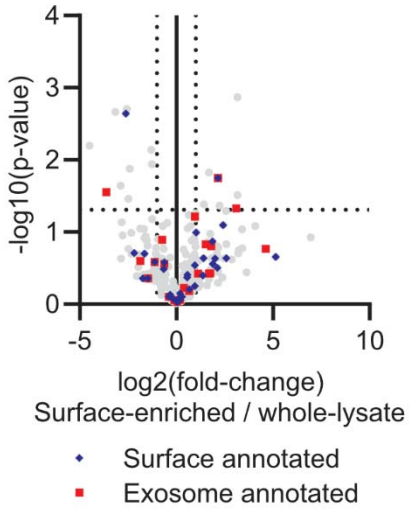

Figure S3. Surface or whole-lysate proteomics of enriched extracellular vesicles does not identify Neu3. Extracellular vesicles from BV-2 microglia were enriched and either lysed (whole-lysate) or subjected to cell surface biotinylation using sulfo-NHS-biotin, followed by lysis and biotin/streptavidin enrichment as described in the materials and methods. Data were quantitated by label-free quantitation. Known surface proteins (blue diamonds) and exosomal proteins (red squares), based on Uniprot GOCC annotation, are labeled.

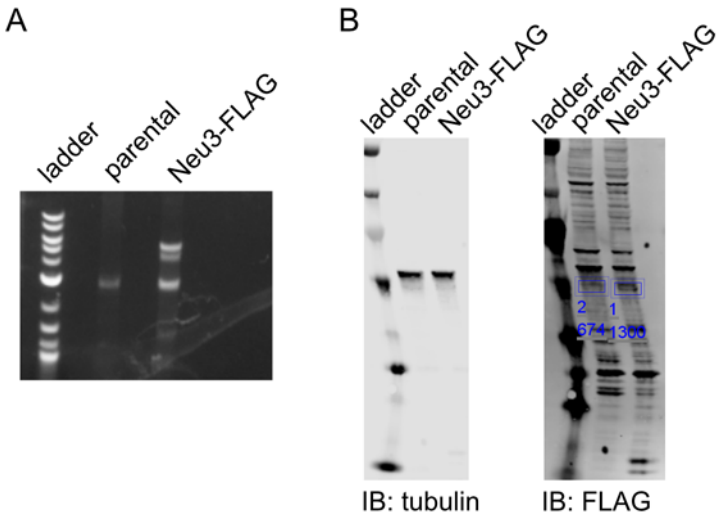

Figure S4. Homology-directed recombination (HDR) produces endogenous Neu3 with a 3xFLAG tag. (A,B) BV-2 microglia were co-transfected with a CRISPR-Cas9 based cutting plasmid and a donor plasmid for HDR to insert the coding sequence for a 3xFLAG tag at the C-terminus of the endogenous *NEU3* gene. (A) PCR of the NEU3 gene shows increased amplicon size in a polyclonal population of transfectants, congruent with tag incorporation. **(B)** Western-blot of whole-cell lysates from parental BV-2 or HDR-transfectants shows a noticeable and quantifiable band in the transfectants at the expected molecular weight of mNeu3.

A

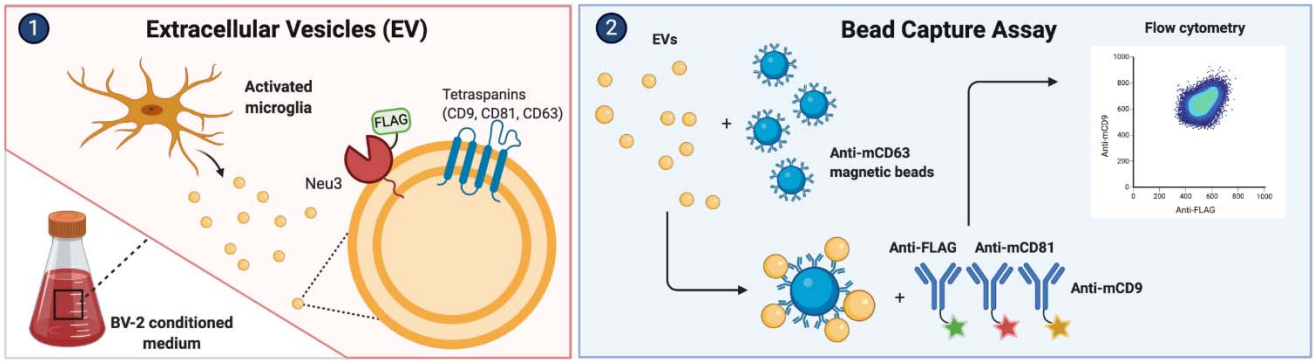
1
Extracellular Vesicles (EV)
Activated microglia
Tetraspanins (CD9, CD81, CD63)
FLAG
Neu3
BV-2 conditioned medium
2
EVs
Bead Capture Assay
Anti-mCD63 magnetic beads
Flow cytometry
Anti-FLAG
Anti-mCD81
Anti-mCD9

B

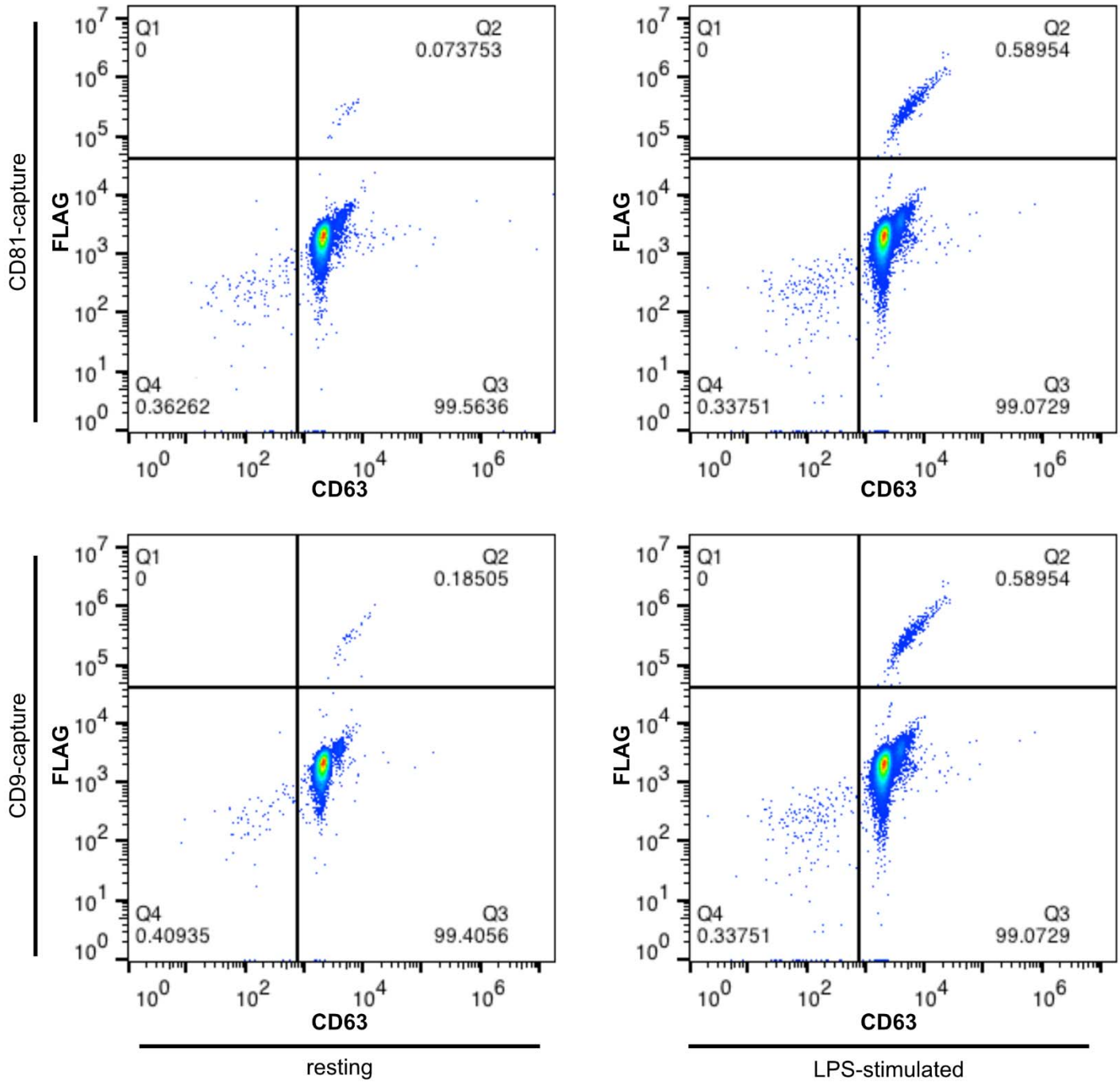
CD81-capture
CD9-capture
FLAG
CD63
Q1
0
Q2
0.073753
Q4
0.36262
Q3
99.5636
Q1
0
Q2
0.58954
Q4
0.33751
Q3
99.0729
Q1
0
Q2
0.18505
Q4
0.40935
Q3
99.4056
Q1
0
Q2
0.58954
Q4
0.33751
Q3
99.0729
resting
LPS-stimulated

Figure S5. LPS-stimulation increases a population of Neu3+ extracellular vesicles in BV-2 microglia. After exposure of BV-2 microglia with endogenously FLAG-tagged Neu3 to vehicle or LPS, EVs were captured on anti-mCD81 or anti-mCD9 coupled beads, labeled with fluorophore-coupled anti-FLAG or anti-mCD63, and analyzed by flow cytometry. **(A)** Representative experimental scheme. **(B)** Representative pseudocolor dot plots from bead-capture experiments in **Figure 2A**.

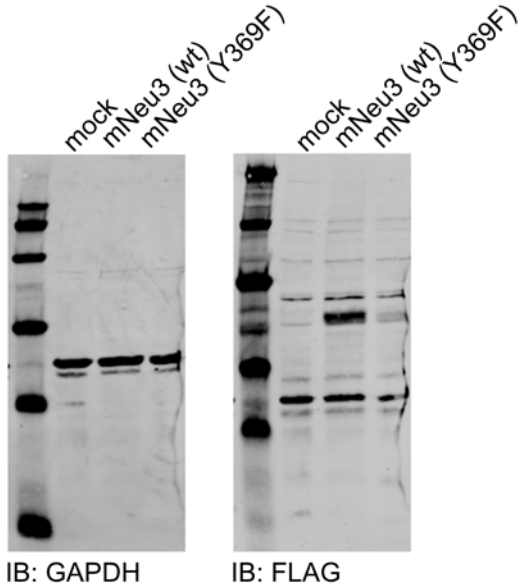

Figure S6. HeLa cells overexpress FLAG-tagged mNeu3 upon transient transfection. HeLa cells were transfected with plasmid encoding either wild-type mNeu3 or a loss-of-function mutant (Y396F) with a C-terminal FLAG tag. Whole cells were lysed and lysates were separated by SDS-PAGE, transferred to nitrocellulose, and probed by Western blot with IR-dye conjugated anti-FLAG or anti-GAPDH antibodies.

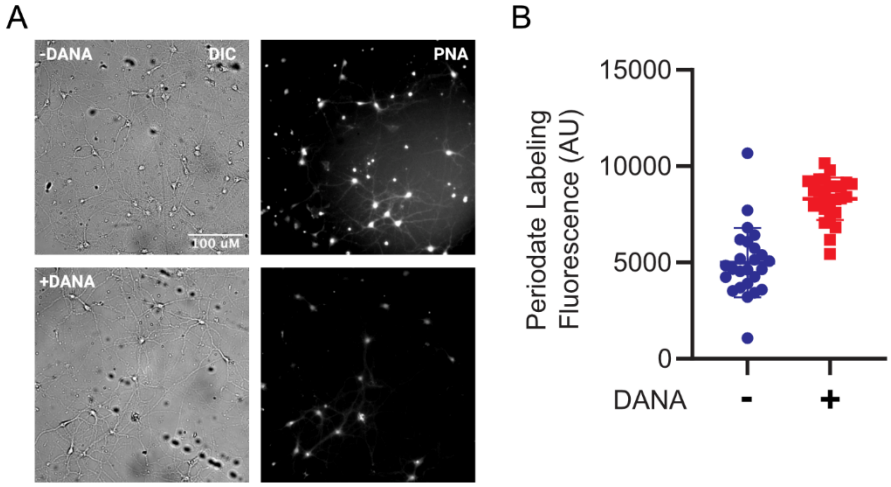

Figure S7. Neu3 on HeLa-derived extracellular vesicles is sufficient to desialylate neurons in culture. Primary mouse hippocampal neurons were treated with conditioned media from NEU3-overexpressing HeLa cells in the presence or absence of deoxy-2,3-anhydroneuraminic acid (DANA). Cell surface sialic acid levels were visualized by periodate labeling. Representative images **(A)** and quantification of fluorescence **(B)** reveal that Neu3 from HeLa-derived extracellular vesicles significantly reduce surface sialic acids (p=0.028) in a sialidase-inhibitor dependent manner. n=3 coverslips/condition, 25 cells/condition.

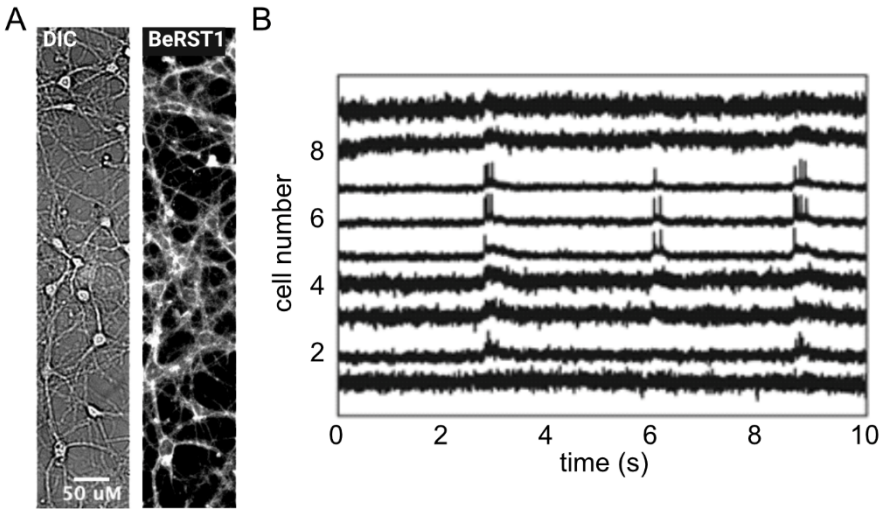

Figure S8. Neu3 on HeLa-derived extracellular vesicles does not produce significant change in firing rate of neurons. Representative images **(A)** and spike traces **(B)** from **Figure 3E** and **3F**.